

GRACEfully closing the water balance: a data-driven probabilistic approach applied to river basins in Iran

Gerrit Schoups¹ and Mohsen Nasseri²

¹Department of Water Management

²School of Civil Engineering

November 24, 2022

Abstract

To fully benefit from remotely sensed observations of the terrestrial water cycle, bias and random errors in these datasets need to be quantified. This paper presents a Bayesian hierarchical model that fuses monthly water balance data and estimates the corresponding data errors and error-corrected water balance components (precipitation, evaporation, river discharge, and water storage). The model combines monthly basin-scale water balance constraints with probabilistic data error models for each water balance variable. Each data error model includes parameters that are in turn treated as unknown random variables to reflect uncertainty in the errors. Errors in precipitation and evaporation data are parameterized as a function of multiple data sources, while errors in GRACE storage observations are described by a noisy sine wave model with parameters controlling phase, amplitude and randomness of the sine wave. Error parameters and water balance variables are estimated using a combination of Markov Chain Monte Carlo sampling and iterative smoothing. Application to semi-arid river basins in Iran yields (i) significant reductions in evaporation uncertainty during water-stressed summers, (ii) basin-specific timing and amplitude corrections of the GRACE water storage dynamics, and (iii) posterior water balance estimates with average standard errors of 4-12 mm/month for water storage, 3.5-7 mm/month for precipitation, 2-6 mm/month for evaporation, and 0-2 mm/month for river discharge. The approach is readily extended to other datasets and other (gauged) basins around the world, possibly using customized data error models. The resulting error-filtered and bias-corrected water balance estimates can be used to evaluate hydrological models.

1 GRACEfully closing the water balance: a data-driven 2 probabilistic approach applied to river basins in Iran

3 G. Schoups¹, M. Nasseri^{2,3}

4 ¹Department of Water Management, Faculty of Civil Engineering and Geosciences, Delft University of
5 Technology, Delft, The Netherlands

6 ²School of Civil Engineering, College of Engineering, University of Tehran, Tehran, Iran

7 ³Visiting Researcher, Department of Water Management, Faculty of Civil Engineering and Geosciences,
8 Delft University of Technology, Delft, The Netherlands

9 **Key Points:**

- 10 A Bayesian hierarchical model fuses water balance data containing unknown bias
11 and random errors
- 12 The model is solved using a combination of Markov Chain Monte Carlo sampling
13 and iterative smoothing
- 14 Computed posteriors provide hydrologically consistent data error and water bal-
15 ance estimates

16 **Abstract**

17 To fully benefit from remotely sensed observations of the terrestrial water cycle, bias and
 18 random errors in these datasets need to be quantified. This paper presents a Bayesian
 19 hierarchical model that fuses monthly water balance data and estimates the correspond-
 20 ing data errors and error-corrected water balance components (precipitation, evapora-
 21 tion, river discharge, and water storage). The model combines monthly basin-scale wa-
 22 ter balance constraints with probabilistic data error models for each water balance vari-
 23 able. Each data error model includes parameters that are in turn treated as unknown
 24 random variables to reflect uncertainty in the errors. Errors in precipitation and evap-
 25 oration data are parameterized as a function of multiple data sources, while errors in GRACE
 26 storage observations are described by a noisy sine wave model with parameters control-
 27 ling phase, amplitude and randomness of the sine wave. Error parameters and water bal-
 28 ance variables are estimated using a combination of Markov Chain Monte Carlo sam-
 29 pling and iterative smoothing. Application to semi-arid river basins in Iran yields (i) sig-
 30 nificant reductions in evaporation uncertainty during water-stressed summers, (ii) basin-
 31 specific timing and amplitude corrections of the GRACE water storage dynamics, and
 32 (iii) posterior water balance estimates with average standard errors of 4-12 mm/month
 33 for water storage, 3.5-7 mm/month for precipitation, 2-6 mm/month for evaporation,
 34 and 0-2 mm/month for river discharge. The approach is readily extended to other datasets
 35 and other (gauged) basins around the world, possibly using customized data error mod-
 36 els. The resulting error-filtered and bias-corrected water balance estimates can be used
 37 to evaluate hydrological models.

38 **1 Introduction**

39 The increasing availability and accuracy of remote sensing data of the terrestrial
 40 water cycle holds great promise for calibration and validation of large-scale hydrologi-
 41 cal models. Several modeling studies have already taken advantage of these data for eval-
 42 uating and constraining hydrological models, including water storage data from GRACE
 43 satellites (L. Zhang et al., 2017; Bai et al., 2018; Scanlon et al., 2018, 2019) and satellite-
 44 based evaporation data (Rientjes et al., 2013; Lopez et al., 2017; Odusanya et al., 2019;
 45 Jiang et al., 2020). A challenge with using remotely sensed data for model evaluation
 46 is that data errors need to be properly accounted for. Data errors are due to e.g. dif-
 47 ferences in scale, errors in the retrieval algorithms, and sensor insensitivities. However,
 48 without a reference "ground-truth" dataset, these errors are difficult to quantify, thereby
 49 undercutting the potential of remote sensing data for advancing large-scale hydrology.
 50 For example, ignoring or misrepresenting systematic data errors (bias) during calibra-
 51 tion leads to biased parameter estimates and limits learning, especially when water bal-
 52 ance data are hydrologically inconsistent, i.e. they do not close the water balance. Fur-
 53 thermore, proper characterization of random errors (noise) and information content of
 54 the data is important: underestimating or even ignoring data noise may lead to overfit-
 55 ting, while overestimating data noise limits learning by not fully exploiting information
 56 content of the data.

57 Processing and use of remotely sensed water balance data therefore requires (i) a
 58 methodology for estimating systematic and random errors in the data, and (ii) a method-
 59 ology that corrects bias, filters out noise, and yields a hydrologically consistent set of wa-
 60 ter balance data that closes the water balance. These are of course well-known challenges,
 61 and the following paragraphs review some of the approaches that have been proposed
 62 in the literature to tackle error estimation and correction of water balance data.

63 A common approach for estimating bias and random data errors of individual wa-
 64 ter balance variables is to compare the data to a reference ground-truth dataset (Moreira
 65 et al., 2019). For example, satellite-based precipitation estimates are often evaluated by
 66 using rain gauge data as ground truth (Beck et al., 2017; Massari & Maggioni, 2020),

67 while errors in evaporation data products have been estimated by comparing to ground-
 68 based measurements from eddy covariance flux towers (Chen et al., 2016; Yang et al.,
 69 2017) and soil moisture sensors (Martens et al., 2017). Another approach to error esti-
 70 mation is to create a reference dataset for the variable of interest by computing it as resid-
 71 ual of the water balance, with all other water balance components assumed known. This
 72 approach has mainly been used for evaporation (Wan et al., 2015; Liu et al., 2016; Weeras-
 73 singhe et al., 2019). Regardless of the approach used for creating the reference dataset,
 74 a conceptual drawback of the "ground-truth" approach is that the "true" values are never
 75 actually measured, since no dataset or estimate is completely error-free. For example,
 76 traditional ground observations, such as rain gauges, are limited in capturing variabil-
 77 ity across large areas, whereas remote sensing data suffer from uncertainties in convert-
 78 ing electromagnetic signals into water balance variable estimates. Nevertheless, in prac-
 79 tice the ground-truth approach may be justified as long as errors in the reference dataset
 80 are sufficiently small relative to the data errors being estimated (Massari & Maggioni,
 81 2020).

82 Alternative error estimation techniques that do not assume a reference ground-truth
 83 dataset have also been developed. The main idea is to use an ensemble of (three or more)
 84 datasets of the same water balance variable, and either estimate errors based on vari-
 85 ability across the ensemble (Tian & Peters-Lidard, 2010; Y. Zhang et al., 2018), or based
 86 on a triple collocation or three-cornered hat method, as has been applied to precipita-
 87 tion (Alemohammad et al., 2015; Massari et al., 2017) and evaporation (Long et al., 2014;
 88 Khan et al., 2018) error estimation.

89 A separate group of studies focuses on bringing together estimates of the different
 90 water balance variables and modifying the original estimates so as to close the water bal-
 91 ance (Pan & Wood, 2006; Sahoo et al., 2011; Pan et al., 2012; Aires, 2014; Munier et al.,
 92 2014; Wang et al., 2015; Allam et al., 2016; Simons et al., 2016; Y. Zhang et al., 2016,
 93 2018; Pellet et al., 2019; Hobeichi et al., 2020). In closing the water balance, variables
 94 with large errors are adjusted more than variables with small errors, a process that can
 95 be formalized by what Pan and Wood (2006) called a constrained Kalman filter. A cru-
 96 cial input of these water balance fusion studies is therefore specification of the magni-
 97 tude of errors in each water balance variable. In existing water balance fusion studies,
 98 error estimates are typically fixed a priori based on expert judgment or on results from
 99 the error estimation techniques mentioned in the previous paragraphs. However, com-
 100 bining error estimates from different studies for water balance closure easily leads to in-
 101 consistencies, e.g. when error estimates of the different variables are based on conflict-
 102 ing underlying ground-truth assumptions, or on data from different regions. Furthermore,
 103 by fixing the data errors in advance, existing water balance fusion studies forego the op-
 104 portunity to improve data error estimates: as we show in this paper, the idea of estimat-
 105 ing errors by bringing together multi-source data, as used in triple collocation for a sin-
 106 gle variable, can also be applied to water balance fusion where data on the different wa-
 107 ter balance variables are combined.

108 The current paper builds on previous efforts and combines the error estimation and
 109 water balance fusion steps into a single methodology that removes the need for a refer-
 110 ence ground-truth dataset. Instead, each water balance variable is assumed to be sub-
 111 ject to unknown bias and random errors, and a single iterative approach is used to es-
 112 timate an internally consistent set of data errors and water balance variables that close
 113 the water balance. The methodology relies on the formulation of a probabilistic model
 114 that combines monthly basin-scale water balance constraints with data error models for
 115 each water balance variable. The data error models relate observations to the underly-
 116 ing unknown true values and contain unknown parameters to account for uncertainty
 117 in the data errors. The overall probabilistic model takes the form of a Bayesian hierar-
 118 chical model with two levels of uncertainty: unknown water balance variables are con-
 119 strained by probability distributions with parameters that themselves are treated as un-

known random variables with specified prior distributions. After conditioning on available water balance data, posteriors of all unknowns, i.e. error parameters and water balance variables, are computed using a combination of Markov Chain Monte Carlo sampling and an iterative form of (Kalman) smoothing. The posteriors automatically fuse all available information and yield best estimates with uncertainty for all water balance variables and error parameters. We note that (Kalman) smoothing, i.e. estimating water balance variables using data from the entire time-series, has not been used in previous water balance fusion studies, which have sometimes used additional postprocessing steps to remove high-frequency artefacts in the estimates (Munier et al., 2014).

The paper starts by introducing the river basins used in this study. Water balance data for these basins is used to motivate development of the probabilistic data error models in section 3. Section 4 details how the probabilistic water balance model is solved, i.e. how posteriors of interest are computed. Section 5 then presents results of applying the methodology to river basins in Iran, followed by an evaluation of different assumptions in the analysis (section 6) and a summary of the main findings.

2 Case study: river basins in Iran

Figure 1 shows locations of the Iranian river basins used in this study. The basins were selected for their availability of river discharge data, their relatively large size, and their geographical location across the country from west to east. Basin boundaries were identified by delineating the topographically upstream areas for each stream gauge providing river discharge data (Table 1). The endorheic Jazmoorian basin drains to an internal lake without natural outlet and hence does not have a stream gauge recording outflow. The basins range in size from 1,600 to 70,000 km² and are generally semi-arid or arid with potential evaporation equal to 1.4 to 5 times average precipitation. Consequently, runoff ratios (Q/P in Table 1) are small, mostly 0.1 or less, with the exception of the relatively steep mountainous Karoon basin. Surface and groundwater withdrawals for irrigation are common and tend to further reduce runoff ratios. All basins have pronounced seasonality in precipitation and runoff, with relatively wet winters and dry summers, translating into seasonal wetting and drying cycles.

The generally water-stressed nature and complex topography of the selected river basins, coupled with significant interventions in the natural water cycle in the form of dams, irrigation, and groundwater pumping, provide a good test-bed for the proposed water balance methodology.

Table 1. River basin characteristics

ID	Basin	Stream gauge (°N, °E)	Area (km ²)	Elevation (m)	$\frac{E_p}{P}^*$	$\frac{Q}{P}^*$
1	Sepidrood	Gilvan (36.83, 49.02)	49246	332-3478	1.78	0.06
2	Karkheh	Abdolkhan (31.83, 48.36)	45497	36-3528	1.61	0.11
3	Karoon	Karoon-IV (32.25, 48.83)	32840	66-4199	1.36	0.38
4	Mond	Ghantareh (28.25, 51.87)	35397	68-3105	2.54	0.04
5	Jazmoorian	(endorheic)	70102	365-4226	5.04	0.00
6	Gorganrood	Bustan Dam (37.42, 55.41)	1620	85-1994	2.04	0.06

* P , Q , and E_p are average precipitation, river discharge and potential evaporation

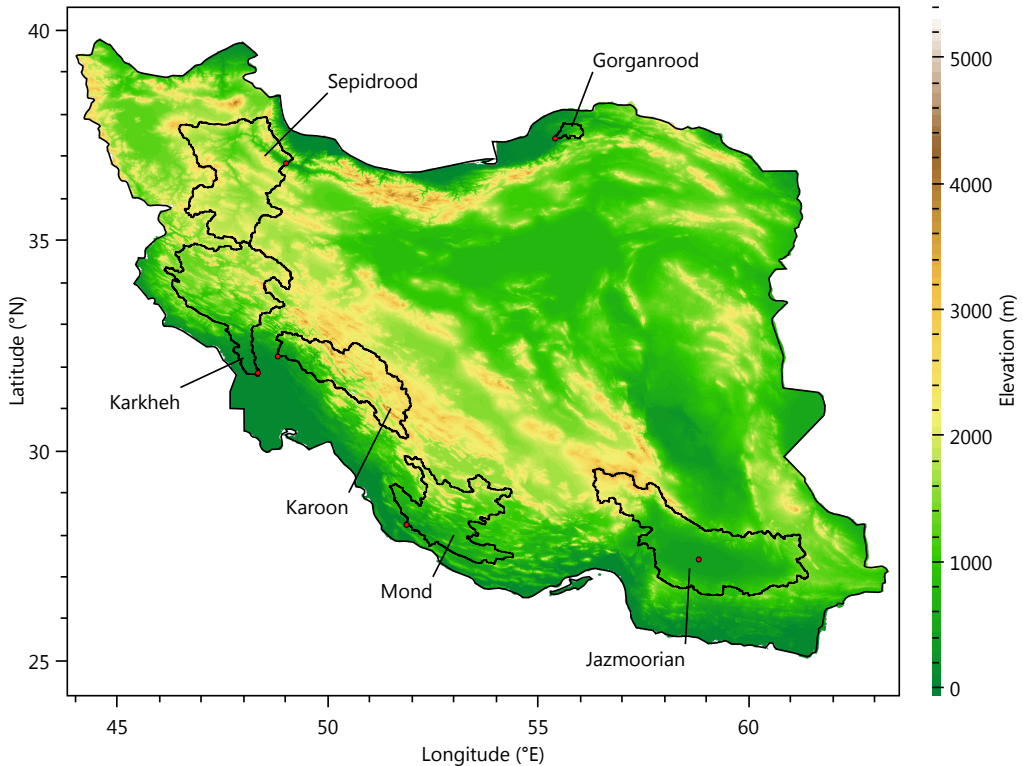


Figure 1. Topographic map of Iran with location of river basins and their outlets.

153 3 Probabilistic water balance model

154 Our interest is in estimating all terms in the monthly basin-scale water balance:

$$155 \quad S_t = S_{t-1} + P_t - E_t - Q_t \quad (1)$$

156 where S_{t-1} and S_t are total water storage (surface and subsurface) in the basin at the
 157 start and end of month t , P_t and E_t are basin average precipitation and evaporation (in-
 158 cluding transpiration), and Q_t is river discharge at the basin outlet for month t . Each
 159 term is normalized by basin area and expressed in consistent water depth units (e.g. mm).
 160 Eq. 1 assumes negligible net lateral groundwater flow into or out of the basin. It also
 161 assumes no significant surface water flows crossing the basin boundary, except for river
 162 discharge at the basin outlet. Thus, upstream inflows and inter-basin water transfers are
 163 considered negligible, although intra-basin water transfers, e.g. via water diversions and
 164 groundwater pumping for irrigation, are captured by Eq. 1. Inter-basin water transfer
 165 is known to occur from the upstream part of Karoon basin (Fig. 1) into the semi-arid
 166 Zayandehrood basin to the north; the transferred amount of water is however negligible
 compared to total runoff in Karoon basin (Abrishamchi & Tajrishy, 2005).

167 In principle, each term in Eq. 1 can be measured or estimated independently. How-
 168 ever, bringing such independent estimates together does not typically lead to water bal-
 169 ance closure, because all measurements and estimates are subject to systematic and ran-
 170 dom errors. Conceptually, it is then useful to distinguish between "true" and "observed"
 171 versions of each water balance variable: by definition, the true water balance variables
 172 close the water balance, and true and observed versions of each water balance variable
 173 are related via data error models that capture systematic and random deviations between
 174 observed and underlying true values.

175 Each data error model consists of parametric probabilistic relations between ob-
 176 served and true values, where parameters quantify the magnitude of systematic and ran-
 177 dom data errors. Since the magnitude of these errors is not known a priori, the param-
 178 eters are themselves treated as random variables with specified prior distributions. The
 179 resulting model can hence be viewed as a Bayesian hierarchical model with two levels
 180 of uncertainty, i.e. one for error parameters and the other for water balance variables.

181 The monthly water balance data used here are summarized in Table 2. We follow
 182 previous water balance fusion studies and focus as much as possible on observational data
 183 instead of hydrological model outputs as source for the water balance data, thereby min-
 184 imizing the impact of hydrological process assumptions. An exception is the GLEAM
 185 evaporation product, which internally relies on a soil water balance model. All data were
 186 spatially averaged across each basin to obtain monthly basin-scale data values. The fol-
 187 lowing sections describe data sources and probabilistic data error models for each wa-
 188 ter balance variable (P , E , Q , S).

Table 2. Monthly water balance data

Variable	Symbol	Data source	Resolution	Reference
Precipitation	P_{obs1}	GPM IMERG Final V06B	0.1°	Huffman et al. (2019)
	P_{obs2}	CHIRPS v2.0	0.05°	Funk et al. (2014)
Evaporation	E_{obs1}	SSEBop v4	0.01°	Senay et al. (2020)
	E_{obs2}	GLEAM v3.3b	0.25°	Martens et al. (2017)
River discharge	Q_{obs}	Stream gauges	Basin	IWRMC (2020)
Storage	S_{obs}	GRACE JPL Mascon RL06v02	3°	Wiese et al. (2018)

189 3.1 Precipitation error model

190 The first dataset used is GPM IMERG (Table 2), which provides monthly precip-
 191 itation values and associated standard errors. Monthly IMERG precipitation merges satellite-
 192 based estimates with the GPCC rain gauge dataset, while standard error estimates are
 193 based on the methodology of Huffman (1997). There is generally a good correspondence
 194 between IMERG and spatially interpolated rain-gauge precipitation for the basins stud-
 195 ied here (Fig. 2, Fig. S1-S2), with the exception of Gorganrood basin. A recent eval-
 196 uation of IMERG across Iran (Maghsoud et al., 2020) reported small but systematic over-
 197 estimation of monthly precipitation in dry regions and underestimation in the wettest
 198 parts of the country. To account for potential bias in IMERG, we included CHIRPS as
 199 a second precipitation dataset. In the semi-arid Mond basin for example (Fig. 2), CHIRPS
 200 tends to give lower precipitation than IMERG during the wet winter months.

201 The following error model was then used to relate observed and true precipitation:

$$m_{P,t} = (1 - w_P)P_{obs1,t} + w_P P_{obs2,t} \quad (2)$$

$$s_{P,t} = \max \left(\sigma_{P,t}, \frac{1}{2} r_P |P_{obs1,t} - P_{obs2,t}| \right) \quad (3)$$

$$P_t \sim \mathcal{N}(m_{P,t}, s_{P,t}^2) \quad (4)$$

$$P_t \geq 0 \quad (5)$$

202 The first equation models bias in the observations by describing prior mean precipita-
 203 tion $m_{P,t}$ in month t as a weighted average of IMERG ($P_{obs1,t}$) and CHIRPS ($P_{obs2,t}$)
 204 monthly basin precipitation. Parameter w_P represents the weight; since it is unknown
 205 a priori, it is given a quasi-uniform prior between 0 and 1 (specifically, a logit-normal

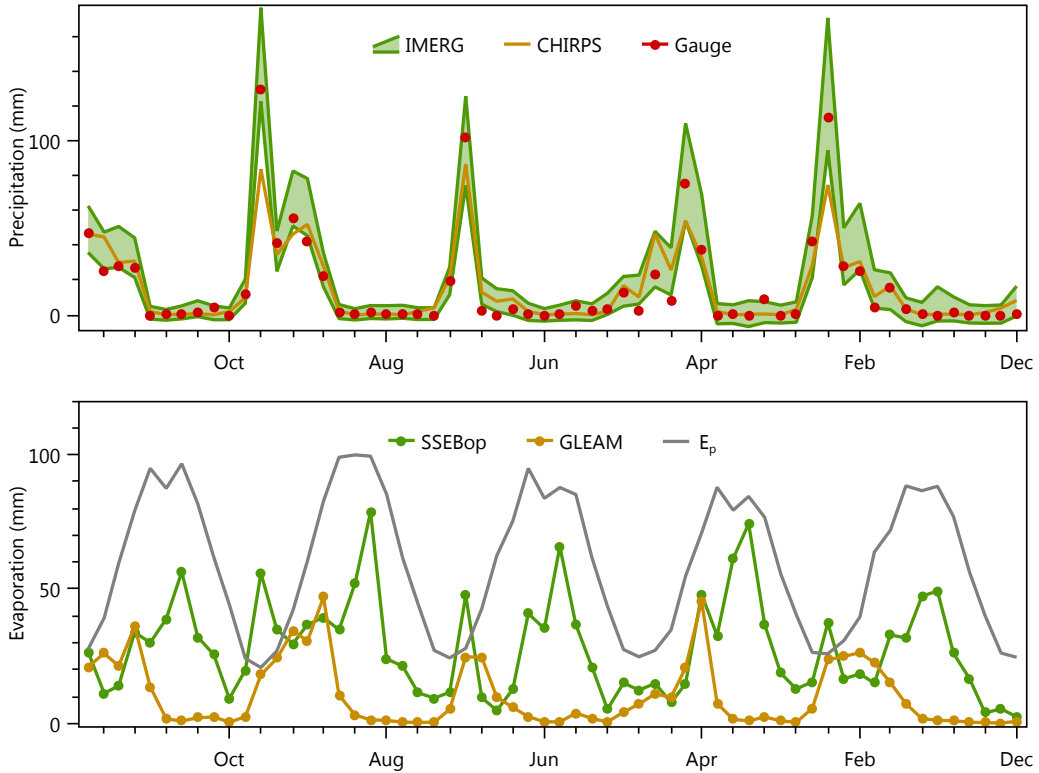


Figure 2. Monthly precipitation and evaporation data for Mond basin during 2006-2010. The IMERG data include standard errors and are plotted as 90% uncertainty bands. Spatially interpolated basin-average rain-gauge precipitation is included for comparison, but was not used in the model. Potential evaporation from the GLEAM dataset is shown as E_p .

prior with location parameter $\mu = 0$ and scale parameter $\sigma = 1.4$) to reflect prior uncertainty about the bias.

The second equation models random errors in the observations by describing prior standard deviation $s_{P,t}$ of precipitation in month t as the largest of either (i) the IMERG standard error $\sigma_{P,t}$, or (ii) the scaled absolute difference between the two precipitation datasets in each month, using r_P as the scaling parameter. The reasoning behind this is that large differences between the two datasets may not only indicate systematic but also significant random errors. Parameter r_P is given a quasi-uniform prior between 0 and 1 to reflect prior uncertainty about the relation between bias and random errors. In the limit when $r_P = 1$, the prior standard deviation is half the absolute difference between the two datasets. However, to avoid unrealistically small prior uncertainty in precipitation, e.g. when r_P is near 0 or the two datasets are in close agreement, the value of $s_{P,t}$ is not allowed to be less than the IMERG standard error $\sigma_{P,t}$. The latter is obtained by arithmetic averaging of the gridded "random error" variable in the IMERG dataset. This implicitly assumes that IMERG random errors are spatially perfectly correlated across the basin. As such, it provides a conservative estimate of the magnitude of basin-scale random errors, since averaging partially uncorrelated grid-scale random errors would result in some error cancellation and therefore smaller values for $\sigma_{P,t}$ at the basin scale.

Finally, the last two equations in the precipitation error model treat true precipitation P_t in month t as a random draw from a truncated normal distribution. Truncation at zero constrains precipitation to be non-negative.

3.2 Evaporation error model

To capture uncertainty and errors in evaporation, two different remote sensing evaporation products are used, i.e. GLEAM and SSEBop (Table 2). These datasets use different methods for estimating evaporation from remote sensing data. GLEAM uses Priestley-Taylor for potential evaporation and estimates actual evaporation as a function of microwave vegetation optical depth and soil moisture, in combination with a root-zone water balance. On the other hand, SSEBop uses Penman-Monteith for potential evaporation and estimates actual evaporation based on a surface energy balance and remotely sensed land surface temperature. For the basins studied in this paper, these two approaches translate into similar evaporation estimates under energy-limited conditions (wet winters), but significantly different evaporation estimates under water-limited conditions (dry summers). Figure 2 illustrates this for the Mond basin, with similar patterns observed in other basins (see Supporting Information): in the absence of significant rainfall during summer, GLEAM evaporation decreases to near-zero values, while SSEBop evaporation shows a peak in summer, suggesting water remains available to natural vegetation or crops (irrigation). These differences result in significant prior uncertainty in evaporation during summers.

A similar error model as for precipitation is adopted for evaporation:

$$m_{E,t} = f_E [(1 - w_E)E_{obs1,t} + w_E E_{obs2,t}] \quad (6)$$

$$s_{E,t} = \max \left(0.1m_{E,t}, \frac{1}{2}r_E |E_{obs1,t} - E_{obs2,t}| \right) \quad (7)$$

$$E_t \sim \mathcal{N}(m_{E,t}, s_{E,t}^2) \quad (8)$$

$$E_t \geq 0 \quad (9)$$

Bias is modeled with two time-invariant parameters: w_E is a weight that interpolates between SSEBop $E_{obs1,t}$ and GLEAM $E_{obs2,t}$ evaporation, and f_E is an additional scaling factor that provides an additional degree of freedom to e.g. account for bias outside the range of the two datasets. Random errors are modeled using the same approach as for precipitation, with parameter r_E controlling to what extent prior uncertainty scales with the absolute difference between the two evaporation datasets. If difference between the two datasets is small, e.g. during energy-limited conditions in winter, a minimum relative error of 10% is assumed by setting $s_{E,t} = 0.1m_{E,t}$. As with precipitation, true evaporation E_t in month t is treated as a random draw from a truncated normal distribution. Truncation at zero constrains evaporation to be non-negative.

Since values of the error parameters are not known a priori, they are given vague prior distributions: quasi-uniform priors between 0 and 1 for w_E and r_E (specifically, flat logit-normal priors between 0 and 1 with location parameter $\mu = 0$ and scale parameter $\sigma = 1.4$), and a log-normal prior for f_E with mode at 1 (no bias) and a coefficient of variation CV of 50%.

3.3 River discharge error model

We assume the basin is gauged and a, possibly incomplete, record of measured monthly river discharge data Q_{obs} is available. A proportional error model is used to relate these

264 data to underlying true discharge values Q :

$$m_{Q,t} = \mathcal{N}(Q_{obs,t}, v_{Q_{obs,t}}) \quad (10)$$

$$s_{Q,t} = a_Q Q_{obs,t} + b_Q \quad (11)$$

$$Q_t \sim \mathcal{N}(m_{Q,t}, s_{Q,t}^2) \quad (12)$$

$$Q_t \geq 0 \quad (13)$$

265 For months with observations, we set $v_{Q_{obs,t}} = 0$, so that the first equation becomes
 266 equivalent to $m_{Q,t} = Q_{obs,t}$, i.e. the mean of Q_t is equal to the (unbiased) observation
 267 for that month. For months with missing observations, $Q_{obs,t}$ and $v_{Q_{obs,t}}$ are set equal
 268 to the mean and variance of river discharge observed for that month across the entire
 269 observation record. This procedure works as long as only a few observations are miss-
 270 ing. For the basins studied in this paper, Gorganrood basin has 1 month with missing
 271 data and Mond basin has 3 months with missing observations.

272 The magnitude of random observation errors is controlled by standard deviation
 273 $s_{Q,t}$, which is modeled as a linear function of the observed discharge for that month (or,
 274 the mean historical discharge for that month in case of a missing observation). This model
 275 assumes that observation errors increase linearly with discharge and includes two time-
 276 invariant parameters, a_Q and b_Q . Parameter a_Q is given a log-normal prior with mode
 277 at 0.1 (i.e. a relative error of 10%) and a small CV of 1%, while b_Q is given a log-normal
 278 prior with mode at 0.001 and also a CV of 1%. Sensitivity of the results to these assumed
 279 narrow priors will be evaluated in section 6.

280 As with precipitation and evaporation, monthly discharge Q_t is constrained to be
 281 non-negative.

282 3.4 Water storage error model

283 The JPL-mascon GRACE water storage data used here (see Table 2) consist of monthly
 284 total terrestrial water storage anomalies relative to the period 2004-2009 at a spatial res-
 285 olution of 3° . The data come post-processed with the Coastline Resolution Improvement
 286 (CRI) filter of Wiese et al. (2016) to reduce leakage errors across land-ocean boundaries.
 287 Figure 3 shows measurement errors of the GRACE data across Iran.

288 Wiese et al. (2016) used simulations with the Community Land Model to down-
 289 scale the coarse 3° storage data to a 0.5° global grid. Here, we use an alternative approach
 290 and instead downscale the data directly to the river basin of interest without using a hy-
 291 drological model: first, the 3° data are weighted-area averaged over each river basin, and
 292 then an error model is specified to quantify systematic and random differences between
 293 the basin-averaged storage data and the true storage changes in the basin.

294 The monthly basin-scale data and true storages both typically have a seasonal cy-
 295 cle, but with possibly different amplitudes and phases, because the coarse-scale data are
 296 polluted by storage dynamics outside of the basin ("leakage"). This motivates the fol-
 297 lowing noisy sine wave error model for quantifying differences between GRACE basin-
 298 scale water storages $S_{obs,t}$ and underlying true storages S_t :

$$m_{S,t} = S_t + A \sin \left(\omega \left(\frac{t}{12} - \delta \right) \right) \quad (14)$$

$$s_{S,t} = \sigma_S \quad (15)$$

$$S_{obs,t} \sim \mathcal{N}(m_{S,t}, s_{S,t}^2) \quad (16)$$

299 Here, A is amplitude (mm), ω is frequency (radians per year), and δ is phase (in years)
 300 of the errors. This model accounts for systematic differences in amplitude and phase be-
 301 tween the observed and true values by means of time-invariant error parameters A and
 302 δ . Furthermore, time-invariant parameter σ_S quantifies magnitude of random errors in

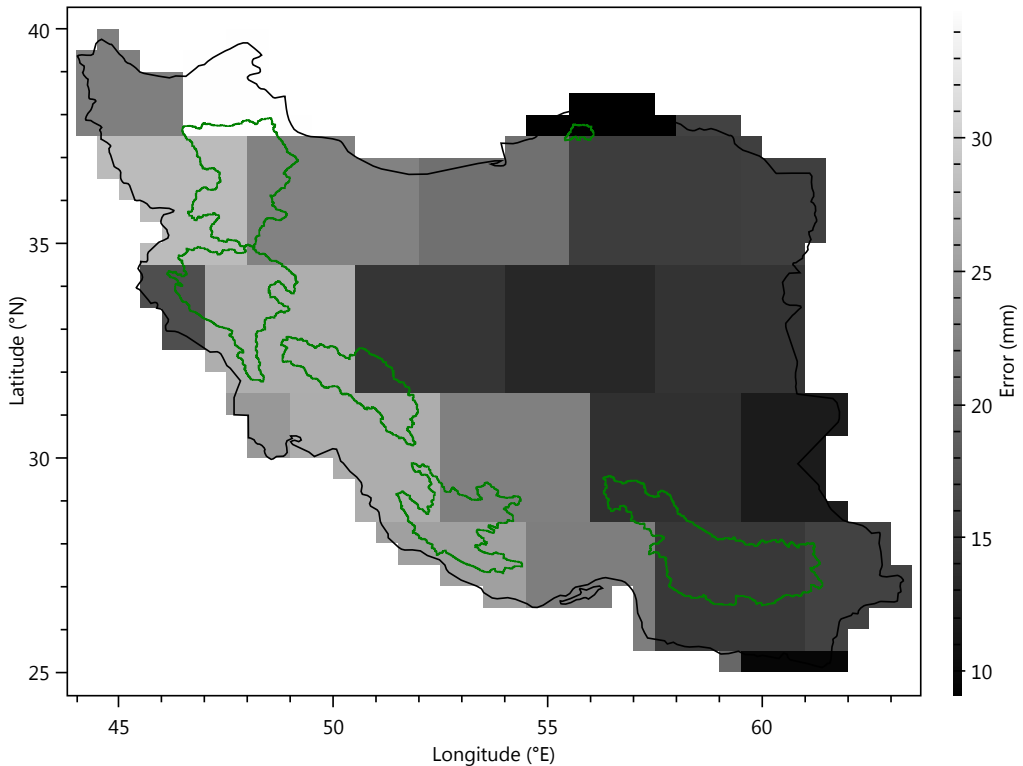


Figure 3. Time-averaged (2006–2015) measurement errors of the JPL GRACE data for each 3° mascon across Iran (based on the "uncertainty" variable in the JPL netcdf dataset). Errors tend to be smaller in arid parts of the country (east and central).

the basin-scale data, which may be caused by (i) inadequacies of the sine wave model and (ii) noise in the GRACE mascon inversion (Wiese et al., 2016), as shown by measurement errors in Fig. 3. We assume here σ_S is unknown and, in section 5, will compare its estimated value for each basin with the measurement errors in Fig. 3.

The value of ω is fixed at 2π radians per year, yielding a sine wave with a 12-month period, while A , σ_S , and δ are given vague priors to reflect prior uncertainty in the values of these parameters. Specifically, A is given a log-normal prior with mode at 30 mm and a CV of 200%, σ_S is given a log-normal prior with mode equal to 10 mm and a CV of 200%, and δ is given a flat logit-normal prior between 0 and 1 year with location parameter $\mu = 0$ and scale parameter $\sigma = 1.4$. Note that parameter δ represents phase of the errors; it should not be interpreted as phase difference between the observed and true signals. For example, if the observed and true signals are in phase, then δ will be equal to the shared phase of these signals, not equal to zero.

Note that the sine wave error model does not include a trend correction: it assumes that any long-term increasing or decreasing trend in the GRACE data is representative for water storage dynamics in the basin. If this assumption is invalid, then this may result in biased posterior estimates for precipitation and evaporation. However, this bias is likely to be relatively small, because water storage trends are sensitive to small changes in precipitation and evaporation. For example, a bias of 1 mm in monthly precipitation adds or removes 120 mm of water over a period of 10 years.

323 While the precipitation and evaporation error models rely on multiple datasets, the
 324 use of multiple GRACE solutions (e.g. the CSR mascon solution (Save, 2020) in addition
 325 to the JPL solution) is not expected to capture prior uncertainty caused by leak-
 326 age or scaling errors, since the different solutions are generally limited by the same coarse
 327 spatial resolution of the GRACE observations. Therefore, the error model uses a single
 328 GRACE solution. Results in section 5 use the JPL data, while the effect of using the CSR
 329 data is evaluated in section 6.

330 4 Inference

331 The probabilistic water balance model described in the previous section defines a
 332 joint distribution over the data and all unknown variables, namely the 10 parameters (w_P ,
 333 r_P , w_E , f_E , r_E , a_Q , b_Q , σ_S , A , δ) and the $4N+1$ monthly water balance variables (S_0 ,
 334 P_t , E_t , Q_t , S_t), where N is the number of months and S_0 is initial basin water storage
 335 at the start of the first month. This paper considers 10 years of data, so $N = 120$. Con-
 336 ceptually, we can write the joint distribution of the model as $p(\mathbf{x}, \boldsymbol{\theta}, \mathbf{S}_{obs})$, where \mathbf{x} rep-
 337 presents all $4N + 1$ water balance variables, $\boldsymbol{\theta}$ is the vector of 10 parameters, and \mathbf{S}_{obs}
 338 represents the entire time-series of storage observations. Formally, this distribution de-
 339 pends on the input observations P_{obs} , E_{obs} , and Q_{obs} , but for notational simplicity this
 340 dependence is omitted here.

341 The goal is now to estimate posterior distributions for \mathbf{x} and $\boldsymbol{\theta}$. The posteriors merge
 342 all available information and data, while accounting for all uncertainties in the model.
 343 We first describe the general form of the posteriors and then discuss the specific infer-
 344 ence algorithm used.

345 4.1 Posterior distributions

346 The posterior for parameter vector $\boldsymbol{\theta}$ can be written as:

$$p(\boldsymbol{\theta}|\mathbf{S}_{obs}) \propto p(\boldsymbol{\theta})p(\mathbf{S}_{obs}|\boldsymbol{\theta}) \quad (17)$$

347 where $p(\boldsymbol{\theta})$ is the prior distribution for the parameters, and $p(\mathbf{S}_{obs}|\boldsymbol{\theta})$ is the likelihood.
 348 The prior is equal to the product of the individual parameter priors defined in the pre-
 349 vious section. The likelihood on the other hand is obtained by computing the normaliz-
 350 ing constant of the conditional water balance posterior $p(\mathbf{x}|\mathbf{S}_{obs}, \boldsymbol{\theta})$, as will be shown
 351 below.

352 The likelihood defines a scoring function for the parameters that quantifies how well
 353 storage predicted from the water balance matches the storage observations \mathbf{S}_{obs} . A good
 354 match can generally be achieved by picking bias parameters (f_E , w_P , etc) that move the
 355 storage predictions closer to the observations, and by making the noise parameters (r_E ,
 356 σ_S , etc) as small as possible: this yields narrow predictive distributions centered on the
 357 observations, and thus large likelihood $p(\mathbf{S}_{obs}|\boldsymbol{\theta})$ for the parameters. However, since the
 358 error parameters are all time-invariant, such near-deterministic predictions generally can-
 359 not be achieved for all months simultaneously. Large likelihood is therefore achieved by
 360 setting the bias parameters to yield a good match on average across the entire time-series,
 361 and setting the noise parameters just large enough to "capture" all observations. Clearly,
 362 many error parameter combinations may yield large likelihood; this non-uniqueness is
 363 captured by characterizing the entire posterior distribution, rather than only determin-
 364 ing the parameters with maximum likelihood or maximum posterior density. As described
 365 in the next section, the parameter posterior distribution is estimated using a Markov Chain
 366 Monte Carlo algorithm.

367 The joint posterior for all water balance variables \mathbf{x} can be written as:

$$p(\mathbf{x}|\mathbf{S}_{obs}) = \int p(\mathbf{x}|\mathbf{S}_{obs}, \boldsymbol{\theta})p(\boldsymbol{\theta}|\mathbf{S}_{obs})d\boldsymbol{\theta} \quad (18)$$

368 where $p(\mathbf{x}|\mathbf{S}_{obs}, \boldsymbol{\theta}) = \frac{p(\mathbf{x}, \mathbf{S}_{obs}|\boldsymbol{\theta})}{p(\mathbf{S}_{obs}|\boldsymbol{\theta})}$ is the posterior distribution of \mathbf{x} , conditioned on spe-
 369 cific values for the parameters. Note that the normalizing constant of this posterior is
 370 equal to the parameter likelihood function $p(\mathbf{S}_{obs}|\boldsymbol{\theta})$ in Eq. 17.

371 Instead of the joint posterior in Eq. 18, we are interested in marginal posterior dis-
 372 tributions $p(x|\mathbf{S}_{obs})$ over individual water balance variables x , where x is a scalar vari-
 373 able equal to one of (S_t , P_t , E_t , Q_t , S_t). For example, if x corresponds to S_t , then we
 374 aim to compute the posterior distribution for S_t based on all observations before, on, and
 375 after time t . Such posterior distributions can be computed, as in Eq. 18, by averaging
 376 conditional posterior distributions $p(x|\mathbf{S}_{obs}, \boldsymbol{\theta})$ over the parameter posterior distribution
 377 $p(\boldsymbol{\theta}|\mathbf{S}_{obs})$. An efficient way of computing all conditional posteriors $p(x|\mathbf{S}_{obs}, \boldsymbol{\theta})$ is to use
 378 a smoothing algorithm, such as a Kalman smoother, as discussed next. Incidentally, a
 379 smoothing algorithm also computes normalizing constant $p(\mathbf{S}_{obs}|\boldsymbol{\theta})$ of $p(\mathbf{x}|\mathbf{S}_{obs}, \boldsymbol{\theta})$, which
 380 is used to compute the likelihood in Eq. 17, without explicitly constructing the $(4N+1)$ -dimensional joint water balance posterior.
 381

382 4.2 Algorithm

383 Following the discussion in the previous section, posterior distributions are com-
 384 puted using a double-loop algorithm that combines Markov Chain Monte Carlo (MCMC)
 385 sampling for the parameter posteriors with Expectation Propagation (EP) (Minka, 2001),
 386 an iterative smoothing algorithm, for the water balance posteriors. Essentially, the MCMC
 387 algorithm forms an outer loop that iteratively proposes and accepts/rejects new param-
 388 eter values, while the EP algorithm forms an inner loop that iteratively computes (i) the
 389 (unnormalized) posterior density, Eq. 17, of parameter values proposed by the MCMC
 390 algorithm, and (ii) conditional water balance posteriors $p(x|\mathbf{S}_{obs}, \boldsymbol{\theta})$ for specific param-
 391 eter vectors sampled by the MCMC algorithm.

392 For linear-Gaussian models, the EP algorithm is equivalent to a Kalman smoother
 393 for S_t , and computes exact Gaussian water balance posteriors via a single forward-backward
 394 pass through the time series, with the backward pass also updating the P_t , E_t and Q_t
 395 posteriors (see Appendix B). The forward-backward pass ensures that water balance pos-
 396 teriors are estimated using data from the entire time-series. Given values for the error
 397 parameters, the probabilistic water balance model in this paper consists of a linear tran-
 398 sition model at each time step (i.e. water balance equation, Eq. 1) with Gaussian stor-
 399 age observations. However, as discussed in the previous section, the model also uses phys-
 400 ical non-negativity constraints for each P_t , E_t , and Q_t . These constraints render the in-
 401 put distributions and water balance posteriors non-Gaussian. The EP algorithm used
 402 here approximates the exact non-Gaussian water balance posteriors with Gaussian dis-
 403 tributions that have the same moments (mean and variance) as the exact posteriors. This
 404 strategy is called moment-matching. Since moment-matching is applied to the posterior,
 405 not the prior, approximations made in one month affect approximations in other months
 406 and the algorithm is iterative: instead of a single forward-backward pass, multiple forward-
 407 backward passes are used, where each pass further refines the approximations until con-
 408 vergence, i.e. until there is no more change in the approximate posteriors.

409 We implement the probabilistic water balance model in C# using the open-source
 410 probabilistic programming library Infer.NET (Minka et al., 2018). The resulting model
 411 code (see Fig. A1) uses the Infer.NET modeling API to implement the model equations
 412 listed in the previous section. This code is then automatically translated by the Infer.NET
 413 compiler into code for running inference, i.e. for computing the water balance posteri-
 414 ors with EP.

415 The MCMC algorithm used in this paper is a single-chain version of the differential-
 416 evolution MCMC algorithm of ter Braak and Vrugt (2008). The algorithm iteratively
 417 proposes new parameter vectors and evaluates their posterior density, Eq. 17, by call-
 418 ing the EP inference code. The latter computation is done in Infer.NET by placing the

419 entire model inside a stochastic if-block and using EP to compute the posterior odds of
 420 being inside vs outside the block, i.e. of the model being "true".

421 Finally, since the EP algorithm only computes conditional water balance posteriors
 422 (conditioned on specific parameter values), a post-processing step is used that av-
 423 erages computed water balance posteriors over the MCMC sampled parameter sets, as
 424 in Eq. 18. That way, the final water balance posteriors account for posterior uncertainty
 425 in the data error parameters. For example, if $p(x|\mathbf{S}_{obs}, \boldsymbol{\theta})$ represents the (Gaussian) pos-
 426 terior for variable x (e.g. E_t), conditioned on data \mathbf{S}_{obs} and on parameter vector $\boldsymbol{\theta}$, then
 427 the final marginal posterior $p(x|\mathbf{S}_{obs})$ is computed from n posterior parameter samples
 428 $\boldsymbol{\theta}_i$ as:

$$p(x|\mathbf{S}_{obs}) = \int p(x|\mathbf{S}_{obs}, \boldsymbol{\theta})p(\boldsymbol{\theta}|\mathbf{S}_{obs})d\boldsymbol{\theta} \approx \frac{1}{n} \sum_{i=1}^n p(x|\mathbf{S}_{obs}, \boldsymbol{\theta}_i) \quad (19)$$

429 As such, each marginal water balance posterior is strictly speaking a (Gaussian) mix-
 430 ture distribution, although empirically it turns out to be well approximated by a single
 431 Gaussian distribution using moment matching. While this last approximation is not strictly
 432 necessary, it avoids storing the entire Monte Carlo mixture (for each water balance vari-
 433 able and each month).

434 5 Results

435 First, detailed results are presented for one of the basins (Mond), followed by a sum-
 436 mary of results for all basins. Detailed results for all basins are available in the Support-
 437 ing Information.

438 5.1 Mond basin

439 Mond basin is one of the drier basins in this study (Table 1). Water balance pos-
 440 teriors for Mond basin are shown in Fig. 4, and error parameter posteriors are shown
 441 in Fig. 5. In Fig. 4, inferred precipitation tends to more closely follow the CHIRPS data
 442 than the IMERG data, especially during the wet winter months, with IMERG appar-
 443 ently overestimating precipitation. This is reflected in the inferred value for parameter
 444 w_P (last row in Fig. 4), which is shifted towards 1, indicating greater weight on CHIRPS
 445 than on IMERG for this basin. The wide posterior for noise scaling parameter r_P indi-
 446 cates that this parameter does not play an important role here, and the posterior un-
 447 certainty in precipitation is not markedly different from the prior uncertainty shown in
 448 Fig. 2.

449 In contrast, posterior uncertainty in evaporation is significantly smaller than its prior
 450 uncertainty, as shown by the posterior uncertainty bands in Fig. 4 (second row) and pos-
 451 terior values of $r_E < 0.5$, indicating that random errors in evaporation are smaller than
 452 the absolute difference between the SSEBop and GLEAM data. Estimated evaporation
 453 lies more or less right between the two datasets, with an estimated w_E value around 0.5
 454 (equal weights) and no additional bias (f_E around 1). Posterior uncertainty increases
 455 during dry summers when differences between the two datasets are largest.

456 River discharge in this basin is an order of magnitude smaller than the other wa-
 457 ter balance variables. With the assumed 10% relative error, this results in small poste-
 458 rior uncertainty that closely follows prior uncertainty (third row in Fig. 4). Note how-
 459 ever the significant increase in discharge uncertainty at the end of the time series: no river
 460 discharge observations are available in the basin for the last three months of 2015, and
 461 historical discharge variability is instead used as prior for these months, as discussed in
 462 section 4. The larger posterior uncertainty in discharge for these months does not ap-
 463 pear to affect uncertainty in the other water balance components. This will be further
 464 explored in section 6.

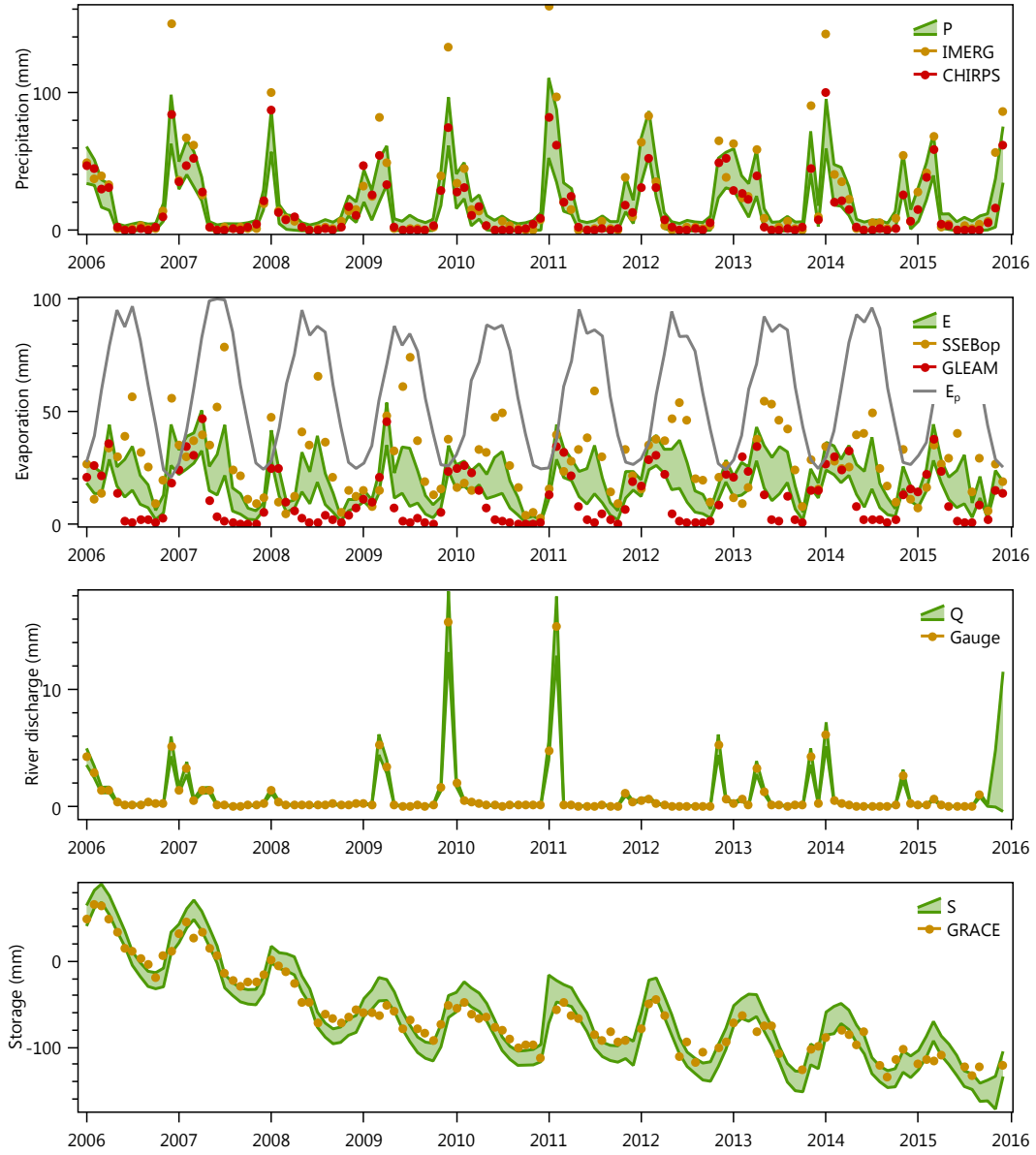


Figure 4. Monthly water balance estimates for Mond basin, shown as 90% posterior uncertainty bands. Each year label indicates start of the year (January). All values are in mm/month.

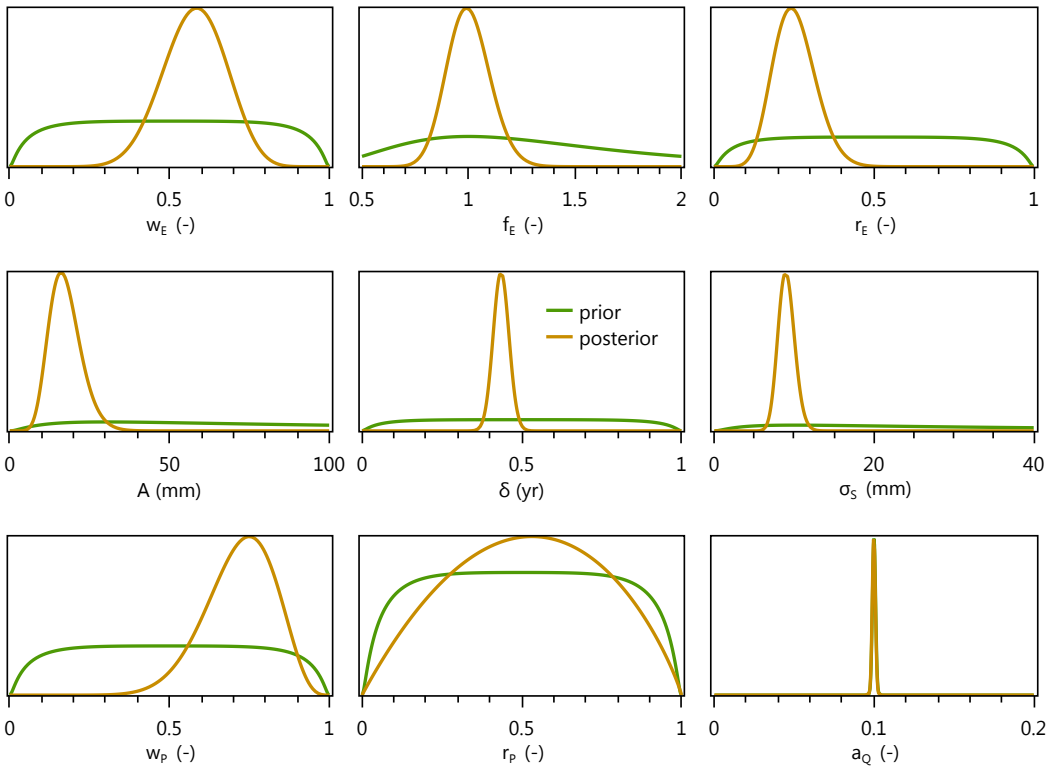


Figure 5. Normalized prior and posterior densities of error parameters for Mond basin.

The last row of Fig. 4 shows that the inferred water storage dynamics largely follow the GRACE observations, with a small increase in seasonal amplitude in the posteriors compared to the data. The corresponding inferred storage error parameters are shown in the second row of Fig. 5. All three parameters (A , δ , σ_S) have well defined posterior distributions compared to their vague priors. Residual noise in the data, after making amplitude (A) and phase adjustments (δ), is relatively small as indicated by an inferred value for σ_S of around 10 mm. Note that inferred posteriors for months with missing GRACE observations (e.g. May-June 2015, October-November 2015) do not markedly differ from months with observations. This is because error parameter values learned from months with data are shared across all months, and because smoothing infers posteriors using data from all months. A more dramatic example of this effect will be seen in section 6.

5.2 Other basins

The Supporting Information contains posterior plots for all other basins, similar to the ones for Mond basin shown above. Here, we highlight the main findings from these results. In terms of water storage posteriors, the basins can roughly be divided into basins without a significant change in amplitude or phase between the estimated posteriors and the GRACE data (Mond, Karoon, Karkheh), basins with only a change in phase (Sepidrood), basins with only a change in amplitude (Jazmoorian), and basins with both a change in amplitude and phase (Gorganrood).

Figure 6 illustrates this for the Sepidrood and Gorganrood basins. In both basins the inferred storage dynamics (posterior shown in green) are shifted earlier in time than the corresponding GRACE observations. Apparently, the observed GRACE dynamics

488 do not fit with the other water balance observations in terms of water balance closure.
 489 Interestingly, both basins are in the north of the country where the large footprint of the
 490 GRACE observations (Fig. 3) is possibly affected by the Caspian Sea to the north, which
 491 is not included in the Coastline Resolution Improvement (CRI) filter of the JPL GRACE
 492 dataset. The sine wave error model appears to restore the underlying water storage dy-
 493 namics, including an increase in amplitude for the relatively small Gorganrood basin.
 494 The increase in amplitude can be explained by the strong spatial smoothing inherent in
 495 the coarse-scale GRACE data, which tends to be more severe in smaller basins.

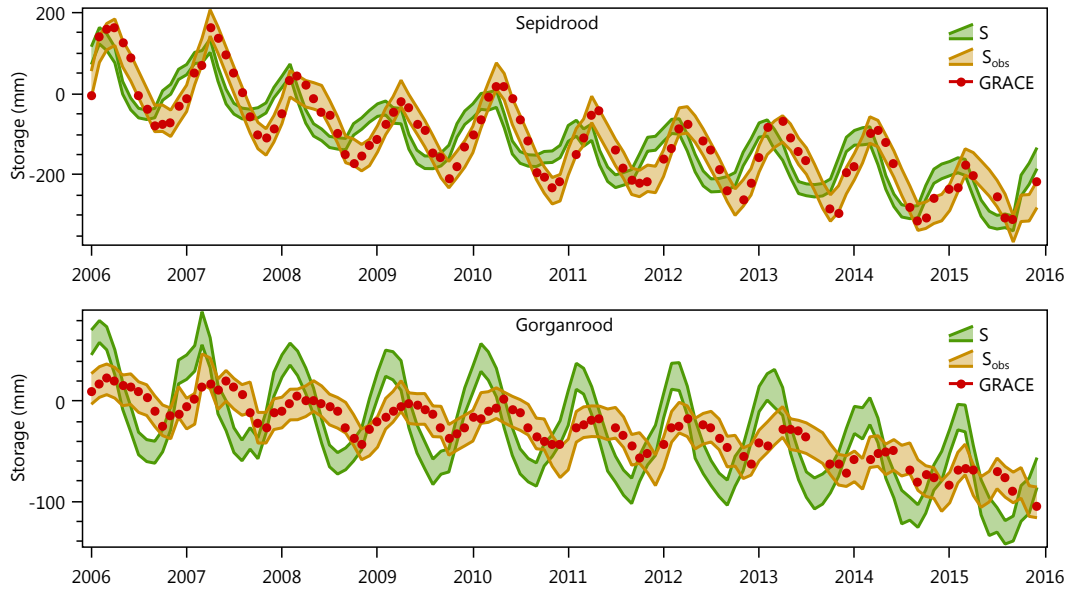


Figure 6. 90% uncertainty bands of storage posteriors (S) and GRACE posterior predictive distributions (S_{obs}), along with GRACE data, for Sepidrood and Gorganrood basins.

496 Fig. 6 also shows posterior predictive distributions for the GRACE observations
 497 (S_{obs}), conditioned on the posterior mean of the true water storage (S). These plots il-
 498 lustrate validity of the proposed sine wave model, since the original GRACE observa-
 499 tions fall within the posterior predictive distributions obtained by taking the inferred pos-
 500 terior mean of S_t in each month and applying the noisy sine wave model to generate a
 501 predictive distribution for the corresponding observation $S_{obs,t}$. This however does not
 502 mean that the probabilistic water balance model is generally suitable for making water
 503 balance predictions, as will be illustrated in section 6.

504 Error parameter posterior distributions for all basins are shown in Fig. 7. The third
 505 row in this figure shows that for most basins IMERG fits better with the other water bal-
 506 ance data than does CHIRPS, since inferred values for w_P are mostly less than 0.5 (more
 507 weight on IMERG). Mond basin is the exception, with $w_P > 0.5$, as discussed above.
 508 The insensitivity of parameter r_P that was already observed in Mond basin, also occurs
 509 in two other basins (Sepidrood and Karkheh), while in the three other basins r_P does
 510 matter and tends toward a value of 1.

511 The three evaporation error parameters are mostly well identified (first row in Fig.
 512 7). In most basins, more weight is given to the GLEAM dataset ($w_E > 0.5$), with the
 513 exception of the wettest basin (Karoon), where SSEBop provides a better fit. However,
 514 in all basins a weighted average of the two datasets is preferred to using either dataset
 515 alone. Inferred values for bias parameter f_E range between 0.5 and 1.5, with the largest

values for Karkheh and Sepidrood basins. While a multiplicative bias of 1.5 may seem excessive, the inferred evaporation posteriors remain at or below potential evaporation (see Supporting Information), even though potential evaporation was not used in the model. Finally, the reduction in prior evaporation uncertainty found in Mond basin also occurs in other basins, as evidenced by inferred values for r_E below 0.5, with the exception of Karkheh and Sepidrood basins, where prior evaporation uncertainty is less pronounced than in the other basins.

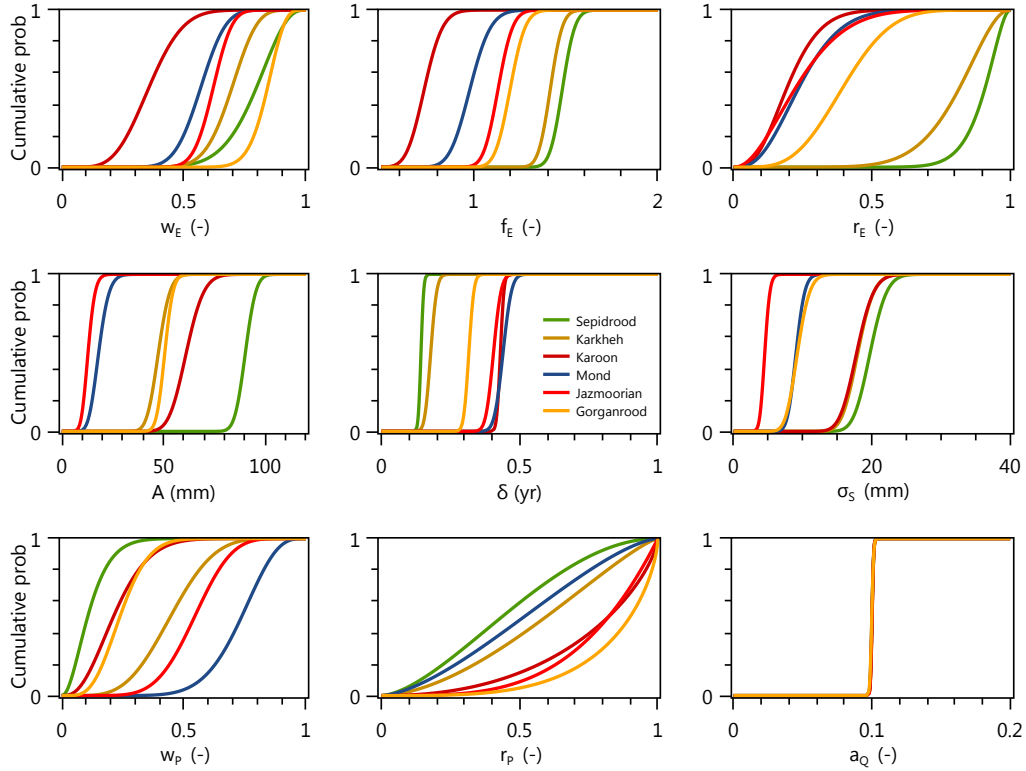


Figure 7. Posterior error parameter distributions for all basins.

The storage error parameters (second row in Fig. 7) are also well identified in all basins. Standard deviation σ_S of random errors in the GRACE observations, after amplitude and phase corrections, is 10 mm or less for the drier basins in the east (Mond, Jazmoorian, Gorganrood) and 15-20 mm for the wetter basins in the west (Sepidrood, Karkheh, Karoon). As shown in Fig. 8, the inferred posterior mean values for σ_S closely follow a similar west-to-east decreasing trend as the JPL-mascon GRACE measurement errors, with an increase in inferred noise for the smaller Gorganrood basin. These results suggest that the sine wave model adequately captured and corrected systematic errors in the GRACE data due to a mismatch in scale, yielding random errors similar to and even smaller than the reported GRACE measurement errors.

Finally, Table 3 summarizes and compares posterior standard deviations for the different water balance variables. The table includes results for a second scenario with vague prior on a_Q , which is further discussed in section 6. Results in this table show that posterior uncertainty, in terms of posterior standard deviation, decreases from water storage (4-12 mm/month), to precipitation (3.5-7 mm/month), to evaporation (2-6 mm/month), and to discharge (0-2 mm/month). The small posterior uncertainty in river discharge is a direct consequence of the assumed 10% error and the generally small discharge val-

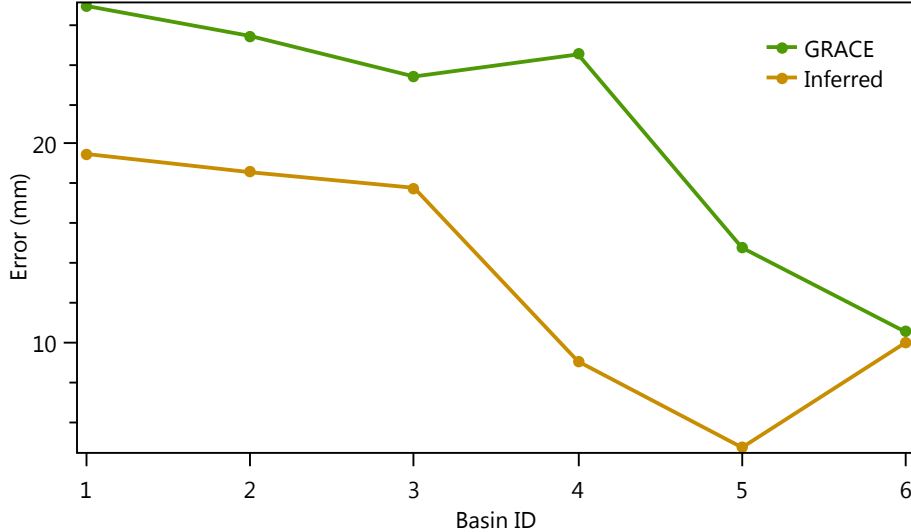


Figure 8. Posterior mean of σ_S compared to mascon-scale standard error of the JPL GRACE observations.

ues in the semi-arid basins studied here. At the extreme end, the endorheic Jazmoorian basin has no outflow, and thus zero discharge and error.

The reported posterior standard deviations result from the fusion of all water balance data. For example, the posterior of S_t in a particular month t results from the fusion of three noisy information streams: the GRACE observation for that month (if not missing), the water balance constraint for month t , and the water balance constraint for month $t + 1$, for which S_t provides the initial storage. Combination of these three information streams results in a posterior that is narrower than any of the individual streams, with each stream or distribution more or less constraining the final posterior estimate of S_t . A similar process happens when inferring the other water balance variables (P_t , E_t , Q_t), although for those variables only two information streams are involved (one from the prior, and the other from the water balance of month t).

Table 3. Average posterior standard deviation (mm/month) of each water balance variable for two cases: (i) relative river discharge error a_Q fixed at 0.1 (10%) and (ii) a vague lognormal prior for a_Q with mode at 0.1 and CV equal to 0.9.

Basin	$a_Q = 0.1$				Vague prior on a_Q			
	P	E	Q	S	P	E	Q	S
Sepidrood	6.0	5.1	0.2	10.1	6.0	5.1	0.4	10.1
Karkheh	6.1	6.1	0.4	11.2	6.2	6.1	1.0	11.1
Karoon	6.9	4.8	1.7	11.3	6.8	4.6	5.6	11.7
Mond	4.7	3.5	0.1	6.7	4.7	3.6	0.3	6.8
Jazmoorian	3.5	1.9	0.0	4.1	3.5	1.9	0.0	4.0
Gorganrood	6.7	4.9	0.2	8.3	6.8	5.0	0.4	8.3

552 **6 Discussion**

553 This section evaluates how results are affected when changing some of the data and
554 assumptions of the probabilistic water balance model.

555 **6.1 Sensitivity to assumed river discharge errors**

556 Results in the previous section were based on a narrow prior for the relative error
557 a_Q of monthly river discharge data centered on 0.1 (10%). To test sensitivity of the re-
558 sults to this choice, an alternative vague lognormal prior for a_Q was used, i.e. one with
559 mode at 0.1 and with a coefficient of variation of 0.9. Table 3 shows that this change in-
560 creases the posterior standard deviation of monthly river discharge, but has otherwise
561 little effect on posterior uncertainty of the other water balance variables. The largest ab-
562 solute increase in posterior standard deviation of Q is observed for Karoon basin, which
563 is the wettest basin included in the analysis. In fact, for Karoon basin, the posterior stan-
564 dard deviation of river discharge becomes larger than that of evaporation (Table 3).

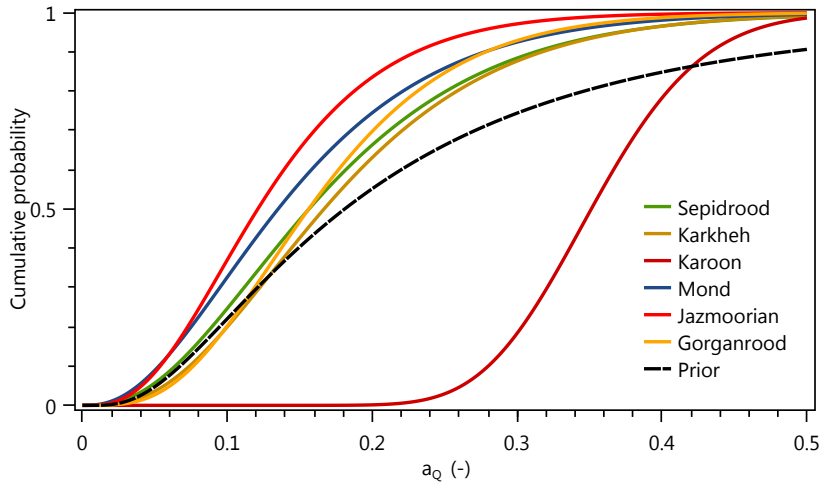


Figure 9. Posterior distributions (cdf) for a_Q when using a vague prior (dashed) for a_Q .

565 When using a vague prior, posterior distributions for relative error a_Q in Fig. 9 show
566 that the posteriors are generally close to the prior. Most basins show a slight contrac-
567 tion of the posterior relative to the prior toward smaller relative errors, with the excep-
568 tion of Karoon basin, where the posterior moves to larger, likely unrealistic, values for
569 a_Q around 0.3–0.4. These large values suggest that uncertainty in river discharge increases
570 to compensate for errors somewhere else in the water balance. Due to the small mag-
571 nitude of river discharge relative to the other water balance terms, a large relative er-
572 ror is needed to get a sizeable effect.

573 These results indicate that, for the semi-arid basins studied here, the value of a_Q
574 cannot reliably be estimated from water balance data, and instead river discharge errors
575 should be estimated independently, e.g. using a formal rating curve error analysis (Horner
576 et al., 2018; Kiang et al., 2018). The value of a_Q can then be fixed a priori, or given a
577 narrow prior, based on the independent estimate. On the other hand, accurate estimates
578 of a_Q are only relevant for estimating uncertainty of the river discharge data. For the
579 goal of estimating the other water balance variables, approximate estimates of a_Q suf-
580 fice, at least when river discharge is the smallest term in the water balance.

581 **6.2 Effect of missing GRACE observations**

582 Results in section 5 already showed that missing GRACE observations do not significantly affect the inferred posteriors. Sharing of error parameters across the entire time-series, combined with fusion of all data via smoothing, allows the model to fill in occasional gaps in the data record. It is however instructive to evaluate a few more drastic
 583 scenarios of missing GRACE observations to gain additional insight into the predictive
 584 capabilities and limitations of the probabilistic water balance model.
 585
 586

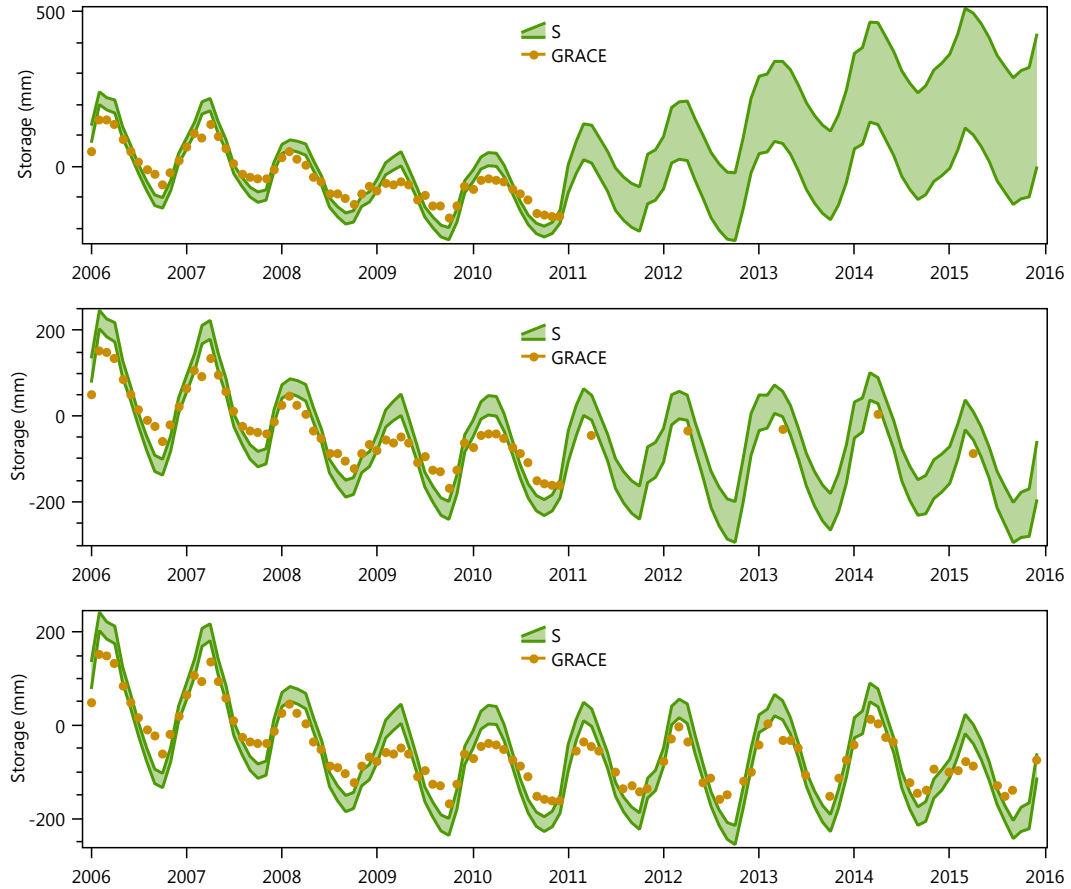


Figure 10. Storage posteriors for Karoon basin for three scenarios of missing GRACE observations: (i) no GRACE observations in the last 5 years, (ii) one GRACE observation per year in the last 5 years, (iii) using all available observations.

588 Two fictitious scenarios are evaluated. The first scenario assumes that all GRACE
 589 observations after 2010 are missing; the first five years provide a complete data record
 590 to learn the model error parameters, which are then applied to infer and predict stor-
 591 age posteriors in the next five years. Fig. 10 shows that in the absence of constraining
 592 GRACE observations in the second part of the period, posterior uncertainty grows over
 593 time, and an increasing trend in storage is (wrongly) predicted. In the second scenario,
 594 which assumes a single annual observation is available after 2010, this trend is removed
 595 and posterior uncertainty is smaller, although it remains larger than when the full GRACE
 596 observation record is used.

These results illustrate that the model is less suitable for long-range predictions without storage observations: uncertainties quickly accumulate, and small imbalances between precipitation and evaporation easily lead to erroneous trend predictions. On the other hand, the model works well for interpolating and filling in gaps when observations are occasionally missing.

6.3 Using a different GRACE solution

The results in this paper are based on the JPL-mascon GRACE data. The model can also use other GRACE solutions by simply replacing S_{obs} in the model by the relevant dataset. Fig. 11 compares inferred posterior distributions for σ_S when using the CSR mascon solution instead of the JPL mascon solution. For the basins studied in this paper, the JPL data consistently yield smaller noise, i.e. smaller posterior values for σ_S . This indicates that the JPL data provide a better fit with the other monthly water balance data used in this study.

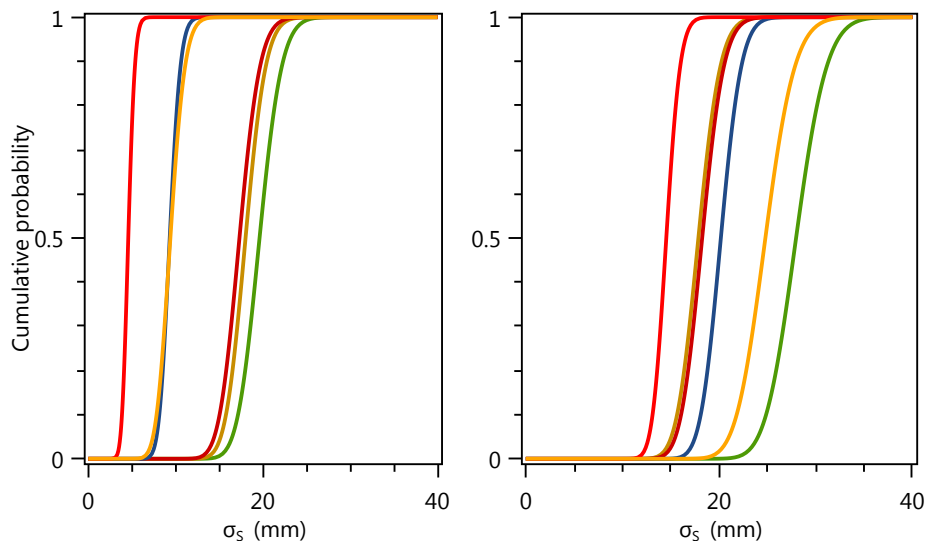


Figure 11. Posterior distributions (cdf) of σ_S for two different GRACE mascon solutions: JPL (left) and CSR (right).

6.4 Effect of positivity constraints

As described in section 4, the model includes positivity constraints on water balance variables P , E , and Q , since these variables cannot physically be negative. To what extent do these constraints affect the inferred posteriors? This can be assessed by removing the positivity constraints from the model, which is achieved by commenting out the three `Variable.ConstrainPositive` statements in Fig. A1) and recomputing the posteriors. Conditional on the model parameters, the model now only contains Gaussian and linear relations. As such, inference does not require any iteration and a single forward-backward pass over the monthly time-series is sufficient to compute all water balance posteriors. The Infer.NET compiler in fact automatically detects this and, in the absence of positivity constraints, generates inference code that is equivalent to a Kalman smoother.

Fig. 12 shows that constraining the water balance variables to be positive results in smaller posterior uncertainty when the unconstrained posterior extends into the neg-

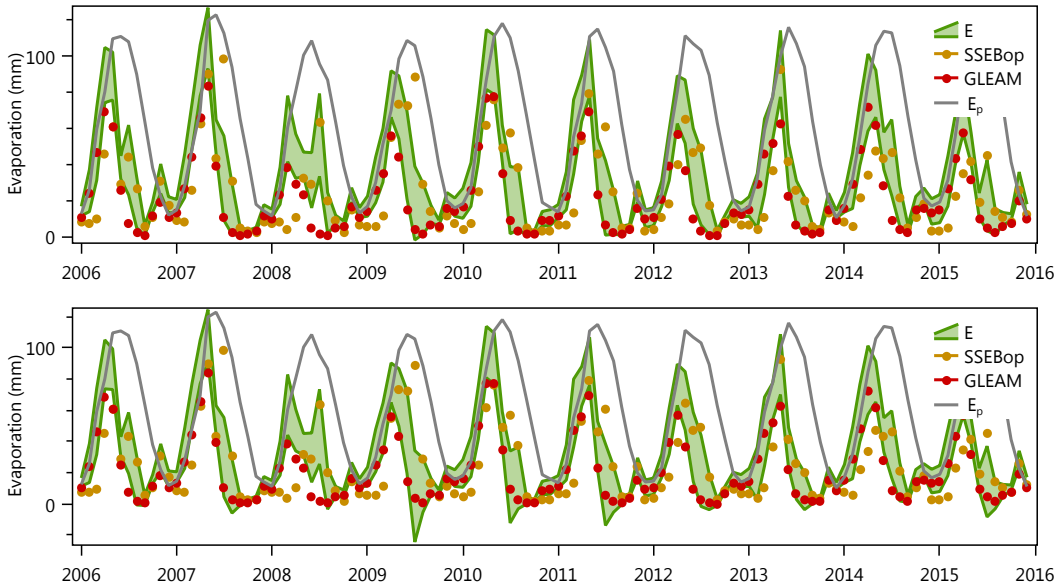


Figure 12. Posterior 90% uncertainty bands for monthly evaporation in Karkheh basin with (top) and without (bottom) positivity constraints in the model.

ative domain. In this case (Karkheh basin), the unconstrained evaporation posterior has a negative tail whenever there is a large difference between the two evaporation datasets (e.g. summer 2009), because then the (prior) uncertainty is large. However, overall for the basins analyzed here, the effect of the positivity constraints is fairly limited and does not significantly change the results. This is also why the number of EP iterations to achieve convergence is small (we used 3 iterations); the studied problems are only mildly non-Gaussian. However, the positivity constraints do maintain physically realistic posteriors and thus are useful for general applicability of the model.

7 Conclusions

The paper presents a probabilistic model to estimate monthly basin-scale precipitation, evaporation, terrestrial water storage and river discharge based on independent observations of each water balance term and monthly water balance constraints. The main contribution compared to previous water balance fusion studies is that data errors are not fixed a priori but are treated as unknown random variables that are estimated from the data. This results in a data fusion approach that combines data error and water balance estimation into a single coherent methodology.

The approach is based on formulating a Bayesian hierarchical model that ties together all data, water balance variables and data error parameters, followed by computing posteriors of all unknown parameters and water balance variables in the model. The model combines monthly basin-scale water balance constraints with data error models for each water balance variable (precipitation, evaporation, river discharge, water storage) that account for random and systematic data errors.

Specifically, bias in precipitation and evaporation data is modeled as a weighted average of two different datasets (IMERG and CHIRPS for precipitation, and SSEBop and GLEAM for evaporation), where the weight is treated as an unknown parameter. For evaporation, a second unknown bias parameter is included for additional flexibility in modeling bias. Random errors in precipitation and evaporation are modeled as a func-

650 tion of differences between the two respective datasets, with unknown parameters
 651 controlling magnitude of the random errors. The JPL-mascon GRACE data are used as basin-
 652 scale water storage observations. Measurement and scaling errors in the GRACE data
 653 are described by a noisy sine-wave error model, with amplitude, phase and noise of the
 654 sine wave controlled by unknown parameters. Finally, monthly river discharge data are
 655 taken from river gauging stations, with random errors described by a relative error pa-
 656 rameter.

657 The resulting probabilistic model is solved for the unknown water balance variables
 658 and data error parameters using Markov Chain Monte Carlo sampling (for the param-
 659 eters) in combination with an iterative smoothing algorithm (for the water balance vari-
 660 ables) that maintains non-negativity of the water balance variables. Computed poste-
 661 riors provide (i) hydrologically consistent, error-filtered and bias-corrected water balance
 662 estimates, and (ii) statistically consistent, basin-specific error estimates of the water bal-
 663 ance data.

664 Application to semi-arid river basins in Iran illustrates usefulness of the approach.
 665 First, computed evaporation posteriors achieve significant reductions in prior evapora-
 666 tion uncertainty during water-stressed summers. Other studies have also reported reduc-
 667 tions in errors by combining multiple evaporation products (Mueller et al., 2011; Hobe-
 668 ichi et al., 2018). Second, the approach leads to basin-specific phase and amplitude cor-
 669 rections of the GRACE data, and is able to extract the underlying water storage dynam-
 670 ics. Third, by fusing all water balance data, posterior water balance estimates are ob-
 671 tained with time-averaged standard errors of 4-12 mm/month for water storage, 3.5-7
 672 mm/month for precipitation, 2-6 mm/month for evaporation, and 0-2 mm/month for river
 673 discharge. Data error parameters are generally well identified, with the exception of rel-
 674 ative error of the river discharge data, which is best estimated using an independent rat-
 675 ing curve analysis. This lack of sensitivity however also means that the other water bal-
 676 ance estimates are not strongly affected by the assumed discharge errors, and an approx-
 677 imate estimate suffices as long as river discharge is the smallest term in the water bal-
 678 ance, as is the case for the semi-arid basins studied here.

679 The proposed methodology is data-driven in that no hydrological process assump-
 680 tions are made beyond the monthly water balance constraints. As such, the water bal-
 681 ance posteriors can be used for independent evaluation and calibration of monthly wa-
 682 ter balance models. Nevertheless, an interesting extension could be to embed the data
 683 errors models used here into a monthly water balance model, and perform joint estima-
 684 tion of all error and hydrological parameters. Another modification would be to consider
 685 spatially distributed error models, e.g. using land cover specific error models for evap-
 686 oration and elevation or temperature specific error models for precipitation, and shar-
 687 ing these parameters across multiple basins to ensure identifiability.

688 The approach can also be extended to other datasets and other (gauged) basins
 689 around the world, possibly using tailor-made data error models. Modifications may be
 690 warranted to describe data errors in different climates and landscapes, e.g. in snow-dominated
 691 basins, where satellite data may underestimate snow accumulation. A benefit in this re-
 692 spect is that the model is implemented in a general-purpose and extensible probabilis-
 693 tic programming tool (Infer.NET) that separates model assumptions from inference (model
 694 solving): when the individual data error models are modified, inference code is automati-
 695 cally generated to compute posteriors for the new model.

696 **Appendix A Implementation of the probabilistic water balance model
697 in Infer.NET**

698 Figure A1 shows how the probabilistic water balance model in section 3 translates
699 directly into a probabilistic program implemented with the Infer.NET modeling API.
700 The Infer.NET compiler automatically translates the model code into an iterative smoothing
701 algorithm for computing water balance posteriors using Expectation Propagation (EP).
The complete code is at <http://doi.org/10.5281/zenodo.4116451>.

```
// Time loop
using (var time = Variable.ForEach(timeInterval))
{
    var t = time.Index;

    // P
    var mP = (1 - wP) * PObs1[t] + wP * PObs2[t];
    var sP = Variable.Max(PStd[t], rP * 0.5 * Abs(PObs1[t] - PObs2[t]));
    P[t] = Variable.GaussianFromMeanAndVariance(mP, sP * sP);
    Variable.ConstrainPositive(P[t]);

    // E
    var mE = fE * ((1 - wE) * EObs1[t] + wE * EObs2[t]);
    var sE = Variable.Max(0.1 * mE, rE * 0.5 * Abs(EObs1[t] - EObs2[t]));
    E[t] = Variable.GaussianFromMeanAndVariance(mE, sE * sE);
    Variable.ConstrainPositive(E[t]);

    // Q
    var mQ = Variable.GaussianFromMeanAndVariance(QObs[t], QObsVar[t]);
    var sQ = aQ * QObs[t] + bQ;
    Q[t] = Variable.GaussianFromMeanAndVariance(mQ, sQ * sQ);
    Variable.ConstrainPositive(Q[t]);

    // S: water balance
    using (Variable.If(t == 0))
    {
        S[t] = S0 + P[t] - E[t] - Q[t];
    }
    using (Variable.If(t > 0))
    {
        S[t] = S[t - 1] + P[t] - E[t] - Q[t];
    }

    // SObs
    var missingSObs = IsNaN(SOBS[t]);
    using (Variable.IfNot(missingSObs))
    {
        const double omega = 2 * Math.PI;
        var mS = S[t] + A * Sin(omega * (Variable.Double(t) / 12 - Delta));
        var sS = SStd;
        SOBS[t] = Variable.GaussianFromMeanAndVariance(mS, sS * sS);
    }
}
```

Figure A1. Implementation of the probabilistic water balance model using the Infer.NET probabilistic programming API in C#.

702

703 **Appendix B Details of EP**

704 Here, we give details of how Expectation Propagation (EP) computes conditional
705 water balance posteriors. EP uses "messages", i.e. Gaussian distributions in this case,

706 to propagate uncertainty through the model. If we write the water balance at each time
 707 as $S = S_0 + P - E - Q$ (omitting time index for simplicity), then the forward message
 708 (Gaussian distribution) to S is computed by propagating Gaussian distributions for the
 709 inputs (S_0, P, E, Q) through the water balance:

$$\text{forward message to } S = \mathcal{N}(S|m_{S_0} + m_P - m_E - m_Q, v_{S_0} + v_P + v_E + v_Q) \quad (\text{B1})$$

710 where m_x and v_x represent mean and variance of input x . Mean and variance of P, E ,
 711 and Q are given by the model priors described in section 3, modified for truncation at
 712 zero, see below. Mean and variance of previous storage S_0 is given by multiplying two
 713 Gaussian distributions: the forward message that was sent to S_0 in the previous time
 714 step and the Gaussian likelihood of a GRACE observation, if any. Mean and variance
 715 of the resulting Gaussian message (distribution) is given by the general Gaussian mul-
 716 tiplication formula:

$$\mathcal{N}(x|m_1, v_1)\mathcal{N}(x|m_2, v_2) \propto \mathcal{N}(x|m, v) \quad (\text{B2})$$

$$m = w_2 m_1 + w_1 m_2 \quad (\text{B3})$$

$$v = w_2 v_1 = w_1 v_2 \quad (\text{B4})$$

717 where $w_1 = \frac{v_1}{v_1 + v_2}$, $w_2 = \frac{v_2}{v_1 + v_2}$, and x in this case would be S_0 . This formula is the
 718 scalar version of the Kalman filter update equation. Forward messages are computed by
 719 a forward pass through the entire time series.

720 Likewise, backward messages represent (Gaussian) distributions that propagate un-
 721 certainty through the model in backward direction. They are computed by a backward
 722 pass through the entire time series, analogous to a Kalman smoother. The backward mes-
 723 sage (Gaussian distribution) to S_0 is computed by propagating Gaussian distributions
 724 for the inputs (P, E, Q) and for S through the water balance back to S_0 :

$$\text{backward message to } S_0 = \mathcal{N}(S_0|m_S - m_P + m_E + m_Q, v_S + v_P + v_E + v_Q) \quad (\text{B5})$$

725 where mean m_S and variance v_S of the backward message from S are obtained by mul-
 726 tiplying the backward message to S (computed in previous step of backward pass) with
 727 the Gaussian likelihood of a GRACE observation, if any, using the same Gaussian mul-
 728 tiplication formula given above. The posterior for each S (or S_0) is obtained by multi-
 729 plying the forward and backward message it receives, as well as a GRACE likelihood mes-
 730 sage, if any.

731 Backward messages to the inputs are computed in a similar way:

$$\text{backward message to } P = \mathcal{N}(P|m_S - m_{S_0} + m_E + m_Q, v_{S_0} + v_S + v_E + v_Q) \quad (\text{B6})$$

$$\text{backward message to } E = \mathcal{N}(E|m_{S_0} - m_S + m_P - m_Q, v_{S_0} + v_S + v_P + v_Q) \quad (\text{B7})$$

$$\text{backward message to } Q = \mathcal{N}(Q|m_{S_0} - m_S + m_P - m_E, v_{S_0} + v_S + v_P + v_E) \quad (\text{B8})$$

732 These backward messages correspond to what Pan and Wood (2006) call a "constrained
 733 Kalman filter". The product of these backward messages and the corresponding priors
 734 gives the posterior for each input. However, since P, E , and Q are constrained to be pos-
 735 itive, the actual posteriors are truncated Gaussians. Moments of each truncated poste-
 736 rior are given by:

$$\mathbb{E}[x^n] = Z^{-1} \int_0^\infty x^n p(x) b(x) dx \quad (\text{B9})$$

737 where x is P, E , or Q , $n = 1, 2$, $p(x)$ is the unconstrained Gaussian prior of x , $b(x)$ is
 738 the backward message to x (Eq. B6-B8), and $Z = \int_0^\infty p(x)b(x)dx$. The posterior is then
 739 approximated by a Gaussian with mean equal to $\mathbb{E}[x]$ and variance equal to $\mathbb{E}[x^2] - \mathbb{E}[x]^2$.
 740 Finally, using a Gaussian division formula analogous to the Gaussian multiplication for-
 741 mula given earlier, the input messages used in Eq. B1 and B5 are computed by divid-
 742 ing the approximate Gaussian posterior by the corresponding backward message $b(x)$.

743 This creates a mutual dependence that is solved by iteration: repeat forward and back-
 744 ward passes over the entire time-series until the approximate posteriors don't change any-
 745 more.

746 Acknowledgments

747 This work was supported by Dutch Research Council (NWO) Visitor Travel Grant no.
 748 040.11.731. Data and code used in this study are available at <http://doi.org/10.5281/zenodo.4116451>.

750 References

- 751 Abrishamchi, A., & Tajrishy, M. (2005). Interbasin water transfers in Iran. In
 752 *Water conservation, reuse, and recycling: Proceedings of an Iranian-American*
 753 *workshop*. National Academies Press.
- 754 Aires, F. (2014). Combining datasets of satellite-retrieved products. Part I: Method-
 755 ology and water budget closure. *Journal of Hydrometeorology*, 15(4), 1677–
 756 1691.
- 757 Alemohammad, S., McColl, K., Konings, A., Entekhabi, D., & Stoffelen, A. (2015).
 758 Characterization of precipitation product errors across the US using multi-
 759 plicative triple collocation. *Hydrology and Earth System Sciences*, 12(2).
- 760 Allam, M. M., Jain Figueroa, A., McLaughlin, D. B., & Eltahir, E. A. (2016).
 761 Estimation of evaporation over the upper Blue Nile basin by combining obser-
 762 vations from satellites and river flow gauges. *Water Resources Research*, 52(2),
 763 644–659.
- 764 Bai, P., Liu, X., & Liu, C. (2018). Improving hydrological simulations by incorporat-
 765 ing GRACE data for model calibration. *Journal of Hydrology*, 557, 291–304.
- 766 Beck, H. E., Vergopolan, N., Pan, M., Levizzani, V., Van Dijk, A. I., Weedon, G. P.,
 767 ... Wood, E. F. (2017). Global-scale evaluation of 22 precipitation datasets
 768 using gauge observations and hydrological modeling. *Hydrology and Earth*
 769 *System Sciences*, 21(12), 6201–6217.
- 770 Chen, M., Senay, G. B., Singh, R. K., & Verdin, J. P. (2016). Uncertainty analy-
 771 sis of the Operational Simplified Surface Energy Balance (SSEBop) model at
 772 multiple flux tower sites. *Journal of Hydrology*, 536, 384–399.
- 773 Funk, C., Peterson, P., Landsfeld, M., Pedreros, D., Verdin, J., Rowland, J., ...
 774 Verdin, A. (2014). A quasi-global precipitation time series for drought
 775 monitoring. *U.S. Geological Survey Data Series 832*. [data.chc.ucsb.edu/](http://data.chc.ucsb.edu/products/CHIRPS-2.0)
 776 *products/CHIRPS-2.0*.
- 777 Hobeichi, S., Abramowitz, G., Contractor, S., & Evans, J. (2020). Evaluating precip-
 778 itation datasets using surface water and energy budget closure. *Journal of Hy-
 779 drometeorology*, 21(5), 989–1009.
- 780 Hobeichi, S., Abramowitz, G., Evans, J., & Ukkola, A. (2018). Derived optimal
 781 linear combination evapotranspiration (dolce): a global gridded synthesis et
 782 estimate. *Hydrology and Earth System Sciences (Online)*, 22(2).
- 783 Horner, I., Renard, B., Le Coz, J., Branger, F., McMillan, H., & Pierrefeu, G.
 784 (2018). Impact of stage measurement errors on streamflow uncertainty. *Water*
 785 *Resources Research*, 54(3), 1952–1976.
- 786 Huffman, G. (1997). Estimates of root-mean-square random error for finite samples
 787 of estimated precipitation. *Journal of Applied Meteorology*, 36(9), 1191–1201.
- 788 Huffman, G., Stocker, E., Bolvin, D., Nelkin, E., & Tan, J. (2019). GPM IMERG
 789 Final Precipitation L3 1 month 0.1 degree x 0.1 degree V06. *Greenbelt, MD,*
 790 *Goddard Earth Sciences Data and Information Services Center (GES DISC)*.
 791 gpm.nasa.gov/data/directory. doi: 10.5067/GPM/IMERG/3B-MONTH/
 792 06
- 793 IWRMC. (2020). *Iran Water Resources Management Company*. <http://wrs.wrm>

- 794 .ir/amar/login.asp.
- 795 Jiang, L., Wu, H., Tao, J., Kimball, J. S., Alfieri, L., & Chen, X. (2020). Satellite-based evapotranspiration in hydrological model calibration. *Remote Sensing*, 12(3), 428.
- 796 Khan, M. S., Liaqat, U. W., Baik, J., & Choi, M. (2018). Stand-alone uncertainty characterization of GLEAM, GLDAS and MOD16 evapotranspiration products using an extended triple collocation approach. *Agricultural and Forest Meteorology*, 252, 256–268.
- 797 Kiang, J. E., Gazoorian, C., McMillan, H., Coxon, G., Le Coz, J., Westerberg, I. K., ... others (2018). A comparison of methods for streamflow uncertainty estimation. *Water Resources Research*, 54(10), 7149–7176.
- 798 Liu, W., Wang, L., Zhou, J., Li, Y., Sun, F., Fu, G., ... Sang, Y.-F. (2016). A worldwide evaluation of basin-scale evapotranspiration estimates against the water balance method. *Journal of Hydrology*, 538, 82–95.
- 799 Long, D., Longuevergne, L., & Scanlon, B. R. (2014). Uncertainty in evapotranspiration from land surface modeling, remote sensing, and GRACE satellites. *Water Resources Research*, 50(2), 1131–1151.
- 800 Lopez, P. L., Sutanudjaja, E. H., Schellekens, J., Sterk, G., & Bierkens, M. F. (2017). Calibration of a large-scale hydrological model using satellite-based soil moisture and evapotranspiration products. *Hydrology and Earth System Sciences*, 21(6), 3125–3144.
- 801 Maghsoud, F. F., Hashemi, H., Hosseini, S. H., & Berndtsson, R. (2020). Ground validation of GPM IMERG precipitation products over Iran. *Remote Sensing*, 12(1), 48.
- 802 Martens, B., Gonzalez Miralles, D., Lievens, H., Van Der Schalie, R., De Jeu, R. A., Fernández-Prieto, D., ... Verhoest, N. (2017). GLEAM v3: satellite-based land evaporation and root-zone soil moisture. *Geoscientific Model Development*, 10(5), 1903–1925.
- 803 Massari, C., Crow, W., & Brocca, L. (2017). An assessment of the performance of global rainfall estimates without ground-based observations. *Hydrology and Earth System Sciences*, 21(9), 4347.
- 804 Massari, C., & Maggioni, V. (2020). Error and uncertainty characterization. In *Satellite precipitation measurement* (pp. 515–532). Springer.
- 805 Minka, T. (2001). *A family of algorithms for approximate Bayesian inference* (Unpublished doctoral dissertation). Massachusetts Institute of Technology.
- 806 Minka, T., Winn, J., Guiver, J., Zaykov, Y., Fabian, D., & Bronskill, J. (2018). *Infer.net 0.3*. (Microsoft Research Cambridge. <http://dotnet.github.io/infer>)
- 807 Moreira, A. A., Ruhoff, A. L., Roberti, D. R., de Arruda Souza, V., da Rocha, H. R., & de Paiva, R. C. D. (2019). Assessment of terrestrial water balance using remote sensing data in South America. *Journal of Hydrology*, 575, 131–147.
- 808 Mueller, B., Seneviratne, S. I., Jimenez, C., Corti, T., Hirschi, M., Balsamo, G., ... others (2011). Evaluation of global observations-based evapotranspiration datasets and ipcc ar4 simulations. *Geophysical Research Letters*, 38(6).
- 809 Munier, S., Aires, F., Schlaffer, S., Prigent, C., Papa, F., Maisongrande, P., & Pan, M. (2014). Combining data sets of satellite-retrieved products for basin-scale water balance study: 2. Evaluation on the Mississippi basin and closure correction model. *Journal of Geophysical Research: Atmospheres*, 119(21), 12–100.
- 810 Odusanya, A. E., Mehdi, B., Schürz, C., Oke, A. O., Awokola, O. S., Awomeso, J. A., ... Schulz, K. (2019). Multi-site calibration and validation of SWAT with satellite-based evapotranspiration in a data-sparse catchment in southwestern Nigeria. *Hydrology and Earth System Sciences*, 23(2).
- 811 Pan, M., Sahoo, A. K., Troy, T. J., Vinukollu, R. K., Sheffield, J., & Wood, E. F. (2012). Multisource estimation of long-term terrestrial water budget for major global river basins. *Journal of Climate*, 25(9), 3191–3206.

- Pan, M., & Wood, E. F. (2006). Data assimilation for estimating the terrestrial water budget using a constrained ensemble Kalman filter. *Journal of Hydrometeorology*, 7(3), 534–547.
- Pellet, V., Aires, F., Munier, S., Jordà, G., Prieto, D., Dorigo, W., ... Brocca, L. (2019). Integrating multiple satellite observations into a coherent dataset to monitor the full water cycle-application to the Mediterranean region. *Hydrology and Earth System Sciences*, 23(1), 465–491.
- Rientjes, T., Muthuwatta, L. P., Bos, M., Booij, M. J., & Bhatti, H. (2013). Multi-variable calibration of a semi-distributed hydrological model using streamflow data and satellite-based evapotranspiration. *Journal of hydrology*, 505, 276–290.
- Sahoo, A. K., Pan, M., Troy, T. J., Vinukollu, R. K., Sheffield, J., & Wood, E. F. (2011). Reconciling the global terrestrial water budget using satellite remote sensing. *Remote Sensing of Environment*, 115(8), 1850–1865.
- Save, H. (2020). CSR GRACE and GRACE-FO RL06 Mascon Solutions v02. doi: [10.15781/cgg9-nh24](https://doi.org/10.15781/cgg9-nh24).
- Scanlon, B., Zhang, Z., Rateb, A., Sun, A., Wiese, D., Save, H., ... others (2019). Tracking seasonal fluctuations in land water storage using global models and GRACE satellites. *Geophysical Research Letters*, 46(10), 5254–5264.
- Scanlon, B., Zhang, Z., Save, H., Sun, A. Y., Schmied, H. M., Van Beek, L. P., ... others (2018). Global models underestimate large decadal declining and rising water storage trends relative to GRACE satellite data. *Proceedings of the National Academy of Sciences*, 115(6), E1080–E1089.
- Senay, G. B., Kagone, S., & Velpuri, N. M. (2020). Operational global actual evapotranspiration: Development, evaluation and dissemination. *Sensors*, 20(7), 1915. earlywarning.usgs.gov/fews/product/460.
- Simons, G., Bastiaanssen, W., Ngô, L. A., Hain, C. R., Anderson, M., & Senay, G. (2016). Integrating global satellite-derived data products as a pre-analysis for hydrological modelling studies: A case study for the Red River basin. *Remote Sensing*, 8(4), 279.
- ter Braak, C. J., & Vrugt, J. A. (2008). Differential evolution Markov chain with snooker updater and fewer chains. *Statistics and Computing*, 18(4), 435–446.
- Tian, Y., & Peters-Lidard, C. D. (2010). A global map of uncertainties in satellite-based precipitation measurements. *Geophysical Research Letters*, 37(24).
- Wan, Z., Zhang, K., Xue, X., Hong, Z., Hong, Y., & Gourley, J. J. (2015). Water balance-based actual evapotranspiration reconstruction from ground and satellite observations over the conterminous United States. *Water Resources Research*, 51(8), 6485–6499.
- Wang, S., Huang, J., Yang, D., Pavlic, G., & Li, J. (2015). Long-term water budget imbalances and error sources for cold region drainage basins. *Hydrological Processes*, 29(9), 2125–2136.
- Weerasinghe, I., Griensven, A. v., Bastiaanssen, W., Mul, M., & Jia, L. (2019). Can we trust remote sensing ET products over Africa? *Hydrology and Earth System Sciences Discussions*, 1–27.
- Wiese, D., Landerer, F. W., & Watkins, M. M. (2016). Quantifying and reducing leakage errors in the JPL RL05M GRACE mascon solution. *Water Resources Research*, 52(9), 7490–7502.
- Wiese, D., Yuan, D., Boening, C., Landerer, F., & Watkins, M. (2018). JPL GRACE mascon ocean, ice, and hydrology equivalent water height, Release 06, Coastal Resolution Improvement (cri) filtered version 1.0. ver. 1.0. *PO.DAAC, CA, USA. grace.jpl.nasa.gov/data*.
- Yang, X., Yong, B., Ren, L., Zhang, Y., & Long, D. (2017). Multi-scale validation of GLEAM evapotranspiration products over China via ChinaFLUX ET measurements. *International Journal of Remote Sensing*, 38(20), 5688–5709.
- Zhang, L., Dobslaw, H., Stacke, T., Güntner, A., Dill, R., & Thomas, M. (2017).

- 904 Validation of terrestrial water storage variations as simulated by different
905 global numerical models with GRACE satellite observations. *Hydrology and*
906 *Earth System Sciences*, 21(2).
- 907 Zhang, Y., Pan, M., Sheffield, J., Siemann, A. L., Fisher, C. K., Liang, M., ... oth-
908 ers (2018). A Climate Data Record (CDR) for the global terrestrial water
909 budget: 1984–2010. *Hydrology and Earth System Sciences*, 22(PNNL-SA-
910 129750).
- 911 Zhang, Y., Pan, M., & Wood, E. F. (2016). On creating global gridded terrestrial
912 water budget estimates from satellite remote sensing. *Surveys in Geophysics*,
913 37(2), 249–268.